A VALIDATION OF GROUND PENETRATING RADAR FOR RECONSTRUCTING THE INTERNAL STRUCTURE OF A ROCK GLACIER: MOUNT MESTAS, COLORADO, USA

A Thesis

by

WILLIAM REVIS JORGENSEN

Submitted to the Office of Graduate Studies of
Texas A&M University
in partial fulfillment of the requirements for the degree of

MASTER OF SCIENCE

May 2007

Major Subject: Geology

A VALIDATION OF GROUND PENETRATING RADAR FOR RECONSTRUCTING THE INTERNAL STRUCTURE OF A ROCK GLACIER: MOUNT MESTAS, COLORADO, USA

A Thesis

by

WILLIAM REVIS JORGENSEN

Submitted to the Office of Graduate Studies of
Texas A&M University
in partial fulfillment of the requirements for the degree of

MASTER OF SCIENCE

Approved by:

Co-Chairs of Committee,	John R. Giardino
	Mark Everett
Committee Member,	Vatche P. Tchakerian
Head of Department,	John H. Spang

May 2007

Major Subject: Geology

ABSTRACT

A Validation of Ground Penetrating Radar for Reconstructing the Internal Structure of a Rock Glacier: Mount Mestas, Colorado, USA. (May 2007)

William Revis Jorgensen, B.S.; B.S., Texas A&M University

Co-Chairs of Advisory Committee: Dr. John R. Giardino
Dr. Mark Everett

Rock glaciers are dynamic landforms and, as such, exhibit interesting and well-developed structural features, which translate to surface morphology in the form of ridges and furrows. These distinguishing features have led researchers to study the physics behind the movement and internal deformation of rock glaciers. For years researchers had no access to the internal makeup of rock glaciers. Thus, proposed models and discussion have been based on theoretical concepts of electromagnetic (EM) wave propogation. With the application of ground penetrating radar (GPR) to provide a view of the interior structure of a rock glacier, researchers had "real" data to verify their models. However, no comparison has been made between a GPR profile and an actual cross-section of a rock glacier. The purpose of this thesis is to validate the fidelity of GPR in showing the actual structure of a rock glacier.

A trench that was excavated through the toe of a rock glacier on Mount Mestas in south central Colorado provided a view of the actual structure of the landform. The structure in the trench was compared with GPR and EM data. The GPR study was conducted using a PulsEKKO^{TM} 100A subsurface imaging radar with 25, 50, and 100

MHz antennas, to detect dielectric contrasts within the rock glacier. A frequency domain EM34 by Geonics Ltd™ was also used to supplement the GPR data by measuring the rock glacier's conductivity at various depths.

This thesis proved, by utilizing statistics, that GPR is a useful tool in visualizing the interior structure of rock glaciers. The 100 MHz antennas clearly show small scale reflection horizons caused by changes in clast orientation and subsurface material composition. These events coincide with structures seen in the trench. Individual clasts greater than 0.375 m were also recognized as point sources in the GPR profiles. Large continuous bedding layers were observed with the 25 and 50 MHz antennas, which reflect the structure seen in the trench. A large scale thrust fault was also located with the GPR. However, this was not visible in the panoramic photograph because the fault occurs below the base of the trench.

DEDICATION

To my parents, Martha and Bill,
for always being there.
Thank you for everything.

ACKNOWLEDGMENTS

I thank my advisor John R. Giardino for providing me with the opportunity of studying and learning with him. I am very grateful for his patience and understanding in the midst of his hectic schedule. I also to thank Mark Everett for the time he spent with me and for sharing his knowledge of geophysics. I especially thank Andrew Nigrini for his willingness to allow me access his property at the rock glacier for the advancement of science. In addition, I thank my friends and field assistants John Degenhardt, Allison Potscavage, Netra Regmi, Douglas Rodriguez, and Rebecca Stokes for their hard work. And lastly, to my mother, Martha, as well as my Aunt Bonnie, who waded through rough draft after rough draft of my manuscript in helping me polish my research communications. Your help was invaluable.

TABLE OF CONTENTS

Page

LIST OF FIGURES

FIGURE Page

LIST OF TABLES

INTRODUCTION AND PROBLEM STATEMENT

Rock glaciers are bodies of frozen debris that are distinctively characterized by surface ridges and furrows, which form perpendicular to the flow direction (Giardino and Vick 1987). These features exist in mountain ranges with debris produced by a microclimate conducive to freeze-thaw cycles (Barsch et al. 1979). Continuous talus supply along with a geographic position and climate that allows sub-zero ground temperatures are necessary for their persistence.

The internal movement of rock glaciers has been a source of speculation by researchers for more than a hundred years (Cross and Howe, 1905; Ostrem, 1971; Barsch, 1977; Giardino, 1979; Martin and Whalley, 1987; Barsch, 1996). These considerations have resulted in lively debates, but none grounded on internal data. The numerous models that have been proposed suggest movement as semi-solid body deformation, thin layer deformation, internal sliding along movement planes, basal sliding, or combinations of all these various mechanisms (Giardino, 1979; Martin and Whalley, 1987; Degenhardt, 2002).

Many methods have been implemented to view the interior structure of rock glaciers. Trenching (Giardino and Vitek, 1988; Zurawek, 2002), borehole measurements (Barsch et al., 1979; Haeberli et al., 1988; Arenson et al., 2002), DC resistivity (Isaksen et al., 2000; Farbrot et al., 2005), Ground Penetrating Radar (Berthling et al., 2000; Degenhardt and Giardino, 2003), and seismics (Potter, 1972; Bucki et al., 2004) have

---

This thesis follows the style and format of Geomorphology.

been used to gain initial information about the interior of several rock glaciers. However, boring and trenching generally are not financially feasible, and they are incredibly invasive techniques. Seismic shot techniques are costly and mildly invasive, hammer-blow seismics is only suitable for limited depth ranges (Sass and Wollny, 2001), and viable access to a study area is required. Ground Penetrating Radar (GPR) is a cost effective, non-invasive, and mobile geophysical method. The frequency range of GPR can vary from less than 1MHz to more than 1GHz, making the equipment adaptable to various near surface conditions. The best sources for data collection should be established on a site-by-site basis.

GPR has been used to examine the internal structure of several rock glaciers (Berthling et al., 2000; Degenhardt and Giardino, 2003; Sauer and Felix-Henningsen, 2004; Degenhardt et al., 2005; Farbrot et al., 2005). Data from these studies indicate continuous reflection horizons throughout the entire length of each rock glacier. These views into the interior of these landforms have aided researchers in their quests to model and explain the internal deformation and movement of these features, but a fundamental question is: how well does the GPR profile mirror the true internal structure of the rock glacier? Unfortunately, comparison of a GPR profile with the actual internal structure has not previously been undertaken. The goal of this research was to ground-truth the usefulness and accuracy of GPR as a tool to map the interior structure of a specific rock glacier. A validation of how accurate the GPR profile matches the internal structure of a rock glacier was needed to achieve this goal.

Supplemental data to verify subsurface anomalies are also desired for the interpretation of the interior of rock glaciers. Electromagnetics (EM) is a means to

measure the conductivity of underlying material. This method is particularly sensitive to bodies of high electrical conductivity, and has been used to delineate faults and shears and in groundwater studies (Sharma, 1997). Supplementing the EM data with GPR profiles can yield both depth and location of the geological anomalies.

For the purpose of this research, GPR surveys were undertaken on a rock glacier on Mount Mestas, Colorado, in 2005 and 2006 as an opportunity to compare GPR profile data with the exposed interior structure. This rock glacier was excavated by the Colorado Highway Department in the 1960s (Johnson, 1967) in search of a borrow source for the construction of a new highway through La Veta Pass. The mountain has been studied in detail by (Patton, 1910), (Giardino, 1976), (Giardino et al., 1978), (Giardino, 1979), (Giardino et al., 1979), (Giardino, 1983), and (Giardino and Vitek, 1988). The ~4.5m wide, ~61 m long, and ~15 m deep excavation provided a window to compare GPR profile data with the actual internal structure of the rock glacier.

Objectives

Ground-truthing the usefulness and accuracy of GPR to map the interior of this rock glacier required four objectives to be established:

- Map the surface morphology of the Mount Mestas rock glacier.
- View the internal structure of the rock glacier using GPR with supplemental EM data.
- Compare the GPR profile and EM data with the exposed trench.
- Confirm GPR data using statistical comparisons.

Completion of these four objectives fulfills the goal and allows answers to the stated problem regarding the accuracy of GPR in mirroring true internal structures of a rock glacier.

MOUNT MESTAS SITE LOCATION AND GEOLOGY

Mount Mestas (37° 35'N, 105° 08'W) is located in Huerfano County in south central Colorado (Figure 1). The mountain is situated 14.2 km (8.8 mi) northwest of the town of La Veta and ~ 32 km (20 mi) west of Walsenburg. Flanked by the North Abyeta Creek and South Abyeta Creek, this mountain has a vertical relief of 1,027 m (3,369 ft), rising from 2,500 m (8,200 ft) in the Abyeta Creek Valley to a summit elevation of 3,526 m (11,569 ft). Mount Mestas is a Tertiary pluton, composed of a homogeneous felsite, which fractures into platy slabs (Giardino and Vitek, 1988), and it forms an easterly extension off of the Sangre De Cristo Formation, an area that is part of the Southern Rocky Mountain system (Giardino, 1979).

The area of this study (Figure 1) is situated on the southeast slopes of Mount Mestas. The mountain is flanked by 44 rock glaciers. The rock glacier selected for study is a typical talus derived tongue-shaped rock glacier, composed of frost-shattered Tertiary felsite. The rock glacier is 800 m in length and ~ 200 m wide, covering an area of ~160,000 m^2. Johnson (1967) noticed interstitial ice within the northern most rock glacier on Mount Mestas in 1963. The ice was encountered at the rock glacier base ~ 10 m in from the toe. He noted that during the summer months, melting ice feeds a small stream which flows down from the toe of the rock glacier. The rock glacier studied does not exhibit either attribute. Whereas ice has not been detected in the toe of this rock glacier, ice has been found in the head of the rock glacier at a depth of 1 m (Giardino, 2006).

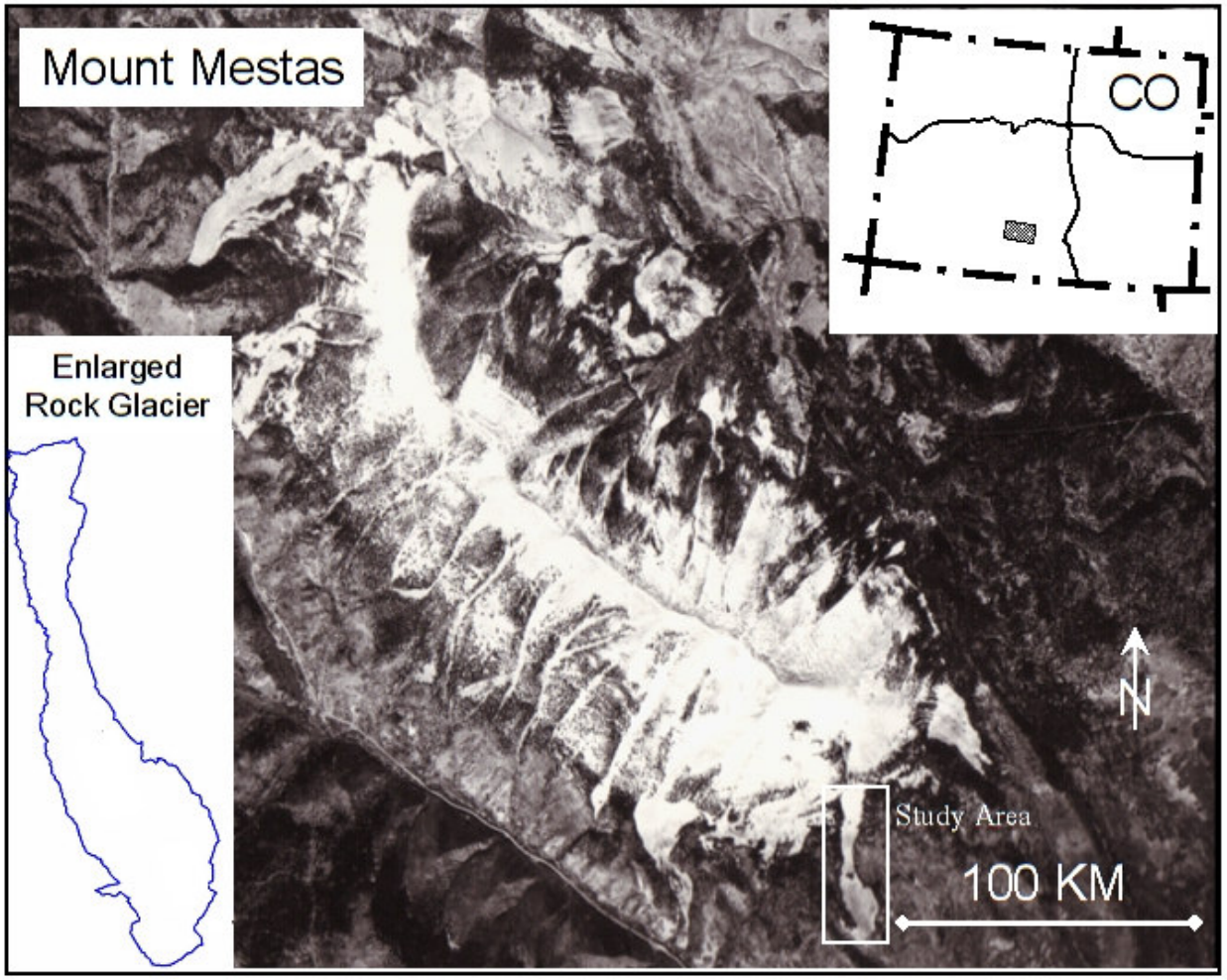

Figure 1. Location and outline of the rock glacier on Mount Mestas.

LITERATURE REVIEW

For years researchers had no access to the internal makeup of rock glaciers. Thus, proposed models and discussion have been based on theoretical concepts of electromagnetic (EM) wave propogation. With the application of ground penetrating radar (GPR) to provide a view of the interior structure of a rock glacier, researchers had "real" data to verify their models.

Researchers have reported that compressional stresses acting on rock glaciers during flow result in surface ridge and furrow development (Giardino, 1979; Haeberli, 1985; Martin and Whalley, 1987; Giardino and Vitek, 1988; Barsch, 1996). It has also been stated that movement is the result of plastic deformation of ice contained within the structure (Haeberli, 1985; Clark, 1988). The compressional stresses and deformation acting on and within rock glaciers can result in an interesting and well developed internal structure consisting of folding, thrust related faulting, and combinations of the two. Various studies have pursued a quest to better understand the inner structure and movement of this dynamic landform.

Giardino (1979) initially studied the causes, mechanics, and rates of movement operating on the surface, within the internal structure, and along the basal contact of various rock glaciers of Mount Mestas in his 1979 dissertation. He studied the external temporal characteristics of rock glaciers and the processes triggering their internal movement. Through the use of fabric analysis obtained from a trench parallel to rock glacier flow, he created two theoretical models for the development of ridges and furrows. His first model suggests movement either by extrusion or shear plane/basal

slippage. It assumes the rock glacier behaves as a plastic body and folds by an accumulation of mass pushing down to form ridges and furrows. The second model suggests that furrows are formed by shear planes created because of a discontinuous presence of interstitial ice; however, Giardino points out that the Mount Mestas rock glaciers are responding to changing conditions and are displaying both random and synchronous patterns of movement.

Martin and Whalley (1987) presented a review of literature on the classification and distribution of rock glaciers in an attempt to simplify the terms used in the extensive writings on this subject. Rock glaciers vary in geographic location and elevational range from the Alaska Range studied by Wahrhaftig and Cox (1959) to the Swiss Alps studied by Barsch and others (1979) to Hamilton Bay, South Georgia (Birnie and Thom, 1982). Ice content within rock glaciers, along with their origin, can vary considerably. Martin and Whalley's paper suggests that confusion exists as to the definition, classification, and interpretation of the significance of rock glaciers.

A structural profile on Mount Mestas was interpreted by Giardino and Vitek (1988) to gain additional information about the mechanics of movement of a rock glacier by using statistical techniques to assess the orientation of clasts in a vertical cross-section. An Eigenvalue procedure was selected for the analysis because the directional frequency can be assessed with a comparison of Eigenvalues. Field measurements were completed by marking lines within the cross section of the rock glacier that separated zones with visually different clast orientations. Dip and strike measurements were acquired on clasts greater than 10 cm. Two hypotheses were postulated on plots of the mean dip of the clasts relative to the land surface, which revealed three cyclic trends. The first hypothesis

implies that catastrophic flow events contributed to the accumulation of debris at the sample site and the morphologic characteristics of the rock glacier, whereas the second hypothesis proposes that the cyclic trends of the clast angle relative to the surface may represent internal slip planes along which rock debris moved.

Berthling and others (2000) studied the internal structure of four rock glaciers in the permafrost zone off the northern Norwegian coast in the arctic, on the island of Prins Karls Forland, western Svalbard, using GPR, and linked those structures to the dynamics and accumulation processes on the rock glaciers. Utilizing 50 MHz antennas oriented transverse to the profile direction, with 1 m spacing, and 0.5 m step size, allowing 1 m resolution, a common structural development along the length of the profile of all studied rock glaciers was observed. Reflectors were parallel with the surface in the upper part of the talus cones (cone shaped accumulations of frost shattered debris from the pluton) above the rock glaciers, but began to dip up against the surface slope down towards the transition to the rock glacier. They concluded that the layering structure is most likely developed by the burial of snow or ice-supersaturated permafrost by large mass movement events. The parallel reflectors along the profile were interpreted to dip up slope relative to the surface. One has to ask: How accurate is the profile in comparison with the actual structure?

Isaksen and others (2000) began investigating the composition, flow, and development of the Hiorthfjellet and Birkafjellet rock glaciers in the permafrost zone of Svalbard in 1994. They attempted to gain a better understanding of the inner structure and the movement of these tongue-shaped rock glaciers to improve the understanding of the developmental processes. By using geodetic surveying techniques, surface velocity

vectors were measured at rates of 0.074 to 0.094 m a^{-1}. The inner structures were studied using both GPR and DC resistivity measurements. GPR antennas of 50 MHz frequency with 2 m spacing were used, oriented perpendicular to the profile direction. One long profile was completed following the central flowline, on two rock glaciers. DC resistivity investigations were undertaken normal to the direction of movement, using an ABEM Terrameter SAS 300 C®, to separate highly resistive layers relative to the lower resistive ice-saturated layers. A four-layer model was used to simplify interpretation.

GPR data were interpreted to represent sediments supersaturated with ice alternating with layers of rockslide debris and can be recognized to a depth of 15 – 20 m. Repeated mass movement events resulting in aggradational ice layers was assumed to be the most important accumulation process for the development of the investigated rock glaciers. Again, the interior structure was interpreted using GPR. But one has to ask: how confident can one be without ground-truthing the use of GPR on rock glaciers?

Farbrot and others (2005) investigated the composition and internal structures of a lobe-shaped rock glacier at Nordenskioldkysten, on the strandflat of western Spitsbergen, Svalbard. Data on composition and internal structures were presented using GPR and DC resistivity tomography measurements. An RAMAC® GPR system from Mala GeoScience was used with antennas of 50 MHz and 1 m separation. One resistivity profile and 2 GPR profiles were obtained. A few continuous radargram profiles were present, but overall the picture appeared to be a chaotic structural pattern. This pattern is assumed to result from an apparent complex history of the rock glacier. Continuous reflection profiles were recorded, however, without a view of the actual cross-section of the rock glacier. Unfortunately, again one has to question the fidelity of acquired data.

Degenhardt and Giardino (2003) investigated the Yankee Boy Rock Glacier in the San Juan Mountains of Colorado using GPR. A conceptual model was developed. Degenhardt and Giardino (2003) also applied this model to interpret similar looking landforms on Mars. Using a PulseEKKO® 100 A radar system, individual transects were collected using 50 MHz and 25 MHz antenna at 2 m and 4 m separation, respectively. The locations of the transects were chosen to identify the gross morphologic and hydrologic characteristics of the rock glacier to determine if a link could be established between internal structure and surface morphology. Results show that the rock glacier is comprised of alternating ice-rich and ice-poor layers. Compressive stresses that originate in the accumulation zone are transmitted downslope and correspond to the surface expression of ridge and furrow topography. Once again, radar traces were interpreted without the aid of GPR ground-truthing.

Fundamental to all these discussions is an effort to gain a better understanding of rock glacier development, movement, and deformation. Even with disagreements over the exact definition of a rock glacier (Martin and Whalley, 1987), there are three certainties:

1) a rock glacier is a body of rock debris that flows down-slope;

2) rock glaciers have a distinctive ridge and furrow morphology;

3) rock glaciers can vary in size, shape, geographic and topographic locations, elevation, origin, activity status, ice content, and geological composition.

To study these largely diversified and structurally complex landforms, researchers need to be creative and technologically aware. Giardino and Vitek (1988) utilized a statistical technique to gain a better understanding of the movement mechanics of rock

glaciers. GPR has been employed by Berthling and others (2000) and Degenhardt and Giardino (2003) to aid in the identification of structural patterns and internal compositions of rock glaciers. Isaksen and others (2000) and Farbrot and others (2005) used both GPR and DC resistivity to interpret and model the internal structure of rock glaciers.

Because of the massive size and hostile acquisition environment associated with studying rock glaciers, the research has its limitations. Most studies run one or two 50 MHz or 25 MHz longitudinal profiles along the flowline, perpendicular to ridges and furrows, to acquire what many think is sufficient data to have a general understanding of the rock glacier in question. Depending on the researcher's goal, it may be monotonous to run grid surveys using both low (25 and 50 MHz) and high frequency (100 or 200 MHz) antennas. Through the use of low frequency antennas, one can locate thick layering and bedrock. High frequency antennas can locate small-scale structural features. More information about the development, movement, and deformation of rock glaciers can be gained by using both low and high frequency antennas.

ROCK GLACIER MECHANICS

To correctly process and interpret GPR data of rock glaciers, knowledge of movement mechanics and structural developments is required. Currently, three types of movement variables have been distinguished in rock glaciers (Haeberli, 1985; Martin and Whalley, 1987; Barsch, 1996). The movement mechanisms include creep of massive ice, creep of interstitial ice, and/or basal shearing (Wahrhaftig and Cox, 1959; Potter, 1972; Giardino, 1979; Giardino and Vick, 1987; Martin and Whalley, 1987; Burger et al., 1999).

Creep is the plastic deformation of the ice in an active rock glacier. It is a function of the amount of mineral component present, the grain size of the minerals, pressure acting on the rock glacier, temperature, and the slope angle that supports the rock glacier. Rates of rock glacier movement increase with increasing temperature and slope angle. The movement rates decrease with increasing mineral grain size and amount of mineral component present.

Basal shearing, stress applied parallel to a surface, assists in the advancement of rock glaciers. This action is believed to be the result of a combination of hydrostatic pressure and lubrication by algae along the rock glacier and valley floor interface (Giardino, 1979). The surface velocity of a rock glacier is greater than the base. This differential velocity with depth creates a distinctive "wrinkled" appearance. Rock glacier velocities vary with depth according to equation 1 (Wahrhaftig and Cox, 1959),

$$\tau_{max} = \gamma H v(\sin t)(\cos t) \qquad (1)$$

where τ_{max} = Basal shear stress, γ = Unit weight, Hv = Vertical thickness, and t = Inclination of the rock glacier's surface with horizontal. Surface ridges and furrows can translate into subsurface folds and faults. By observing the surface morphology, assumptions can be made about the interior structure.

In a previous study, Giardino (1979) proposed two theoretical models for the development of ridges and furrows (Figures 2 and 3). As material and pressures build up on the head of a rock glacier, the head compresses towards its toe. The rock glacier deforms plastically to accommodate the increasing forces and surface area in the form of folds and faults. As the rock glacier moves, deformation takes place, which is very typical of large and small-scale tectonics. In the first model, Figure 2, ridges and furrows are formed by fault-propagation folding. In fault-propagation folding, strata cut by the base of the ramp are shortened by thrusting (Figure 4). In Figure 4, two arrows along the ramp show the hanging wall moves up relative to the footwall, the ramp and fault tip are noted, and the direction of compression and propagation is revealed. Strata above the tip of the fault are shortened entirely by folding. Intermediate strata are shortened by a combination of both folding and faulting.

The second proposed model gives fault-bend folding as the main deformation mechanism for the formation of ridges and furrows on rock glaciers (Figure 3). Fault-bend folds are a consequence of compressional forces. Fault-bend folding is the process by which fault blocks are folded as they pass over bends in faults. A model of this process is shown in Figure 5. The thrust plane comes from the right, cuts upward across bedding, and continues parallel with bedding off to the left. Because layers must conform to changing fault geometries, folding occurs. Ridges increase in displacement

until a point of maximum threshold causes the ridge to overturn on top of the underlying furrow, as shown by the fold axis (Giardino, 1979).

By knowing and understanding theoretical movement mechanics and structural developments on and within rock glaciers, an interpretation of GPR profiles can be made. Many forces act on rock glaciers simultaneously, creating a combination of structural variations throughout. The movement mechanics and theoretical models for the development of ridges and furrows give the researcher a foundation to build.

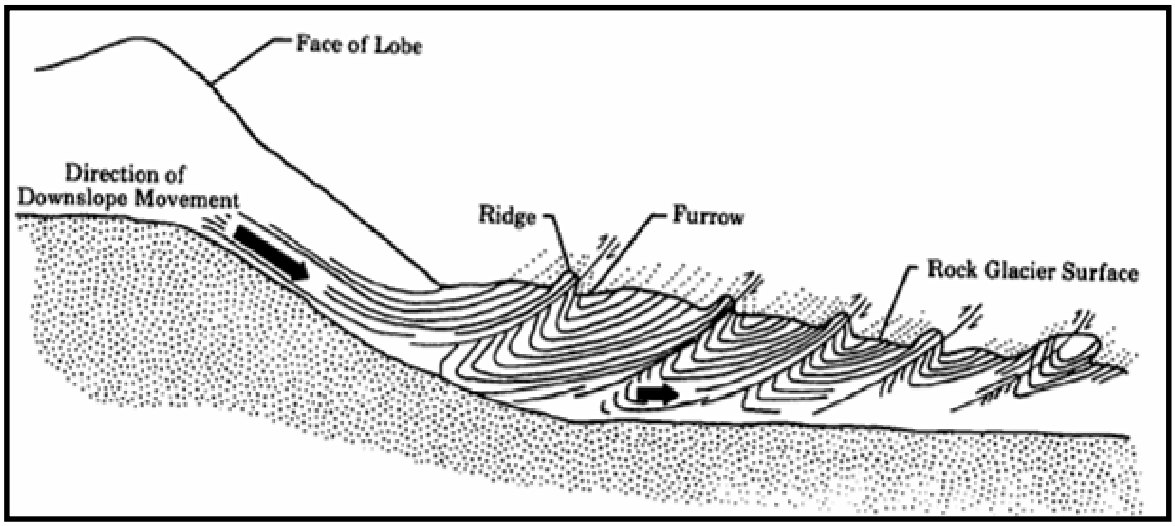

Figure 2. Ridge and furrow development through fault-propogation folding (Giardino, 1979).

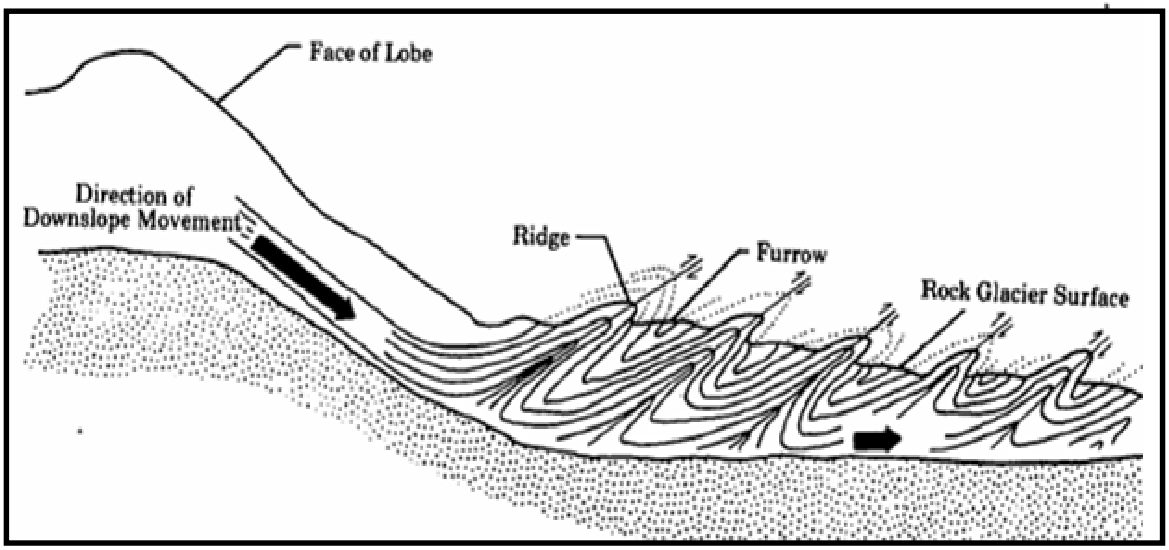

Figure 3. Ridge and furrow development through fault-bend folding (Giardino, 1979).

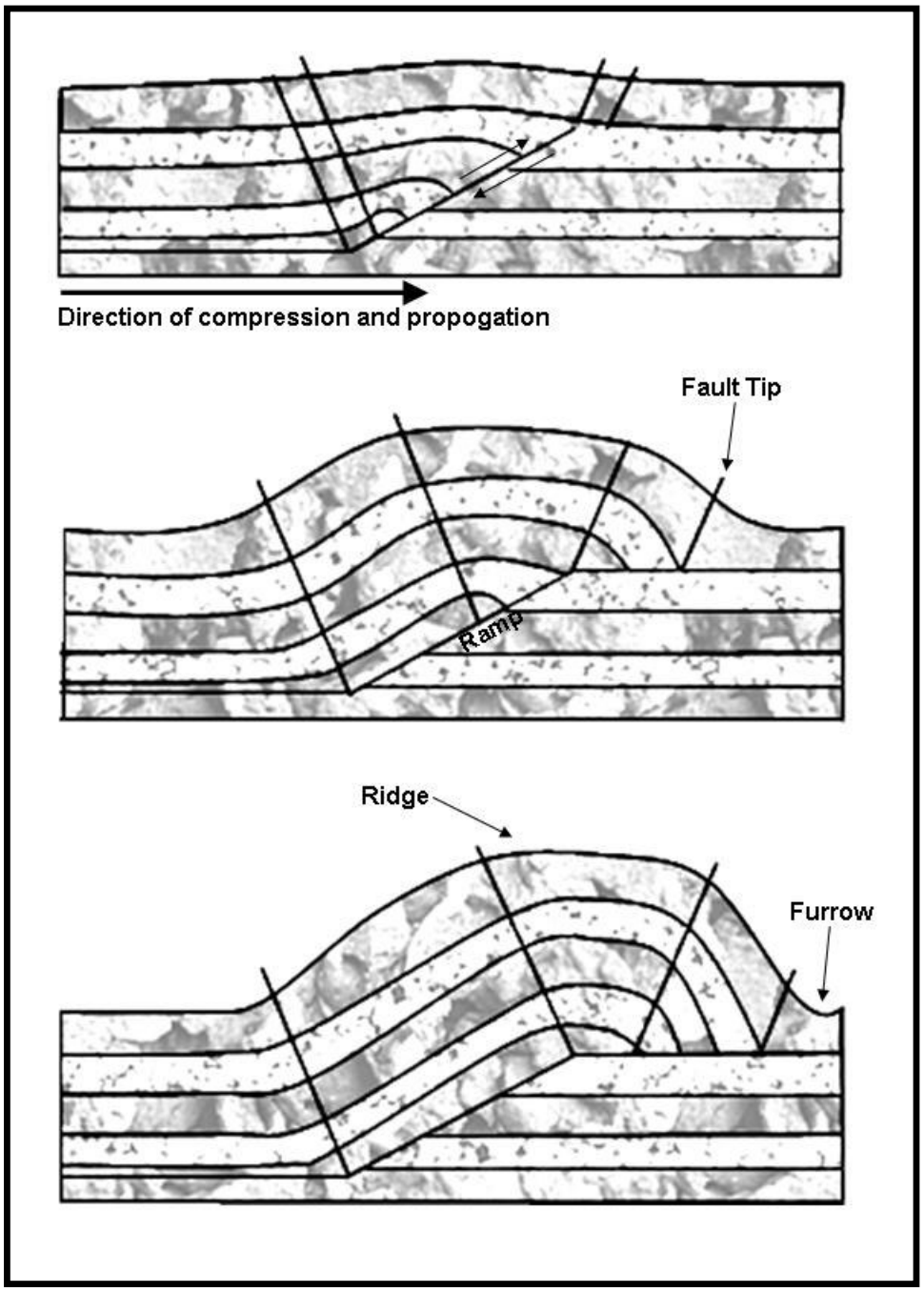

Figure 4. Fault-bend folding diagram (Modified after Pollard 2005).

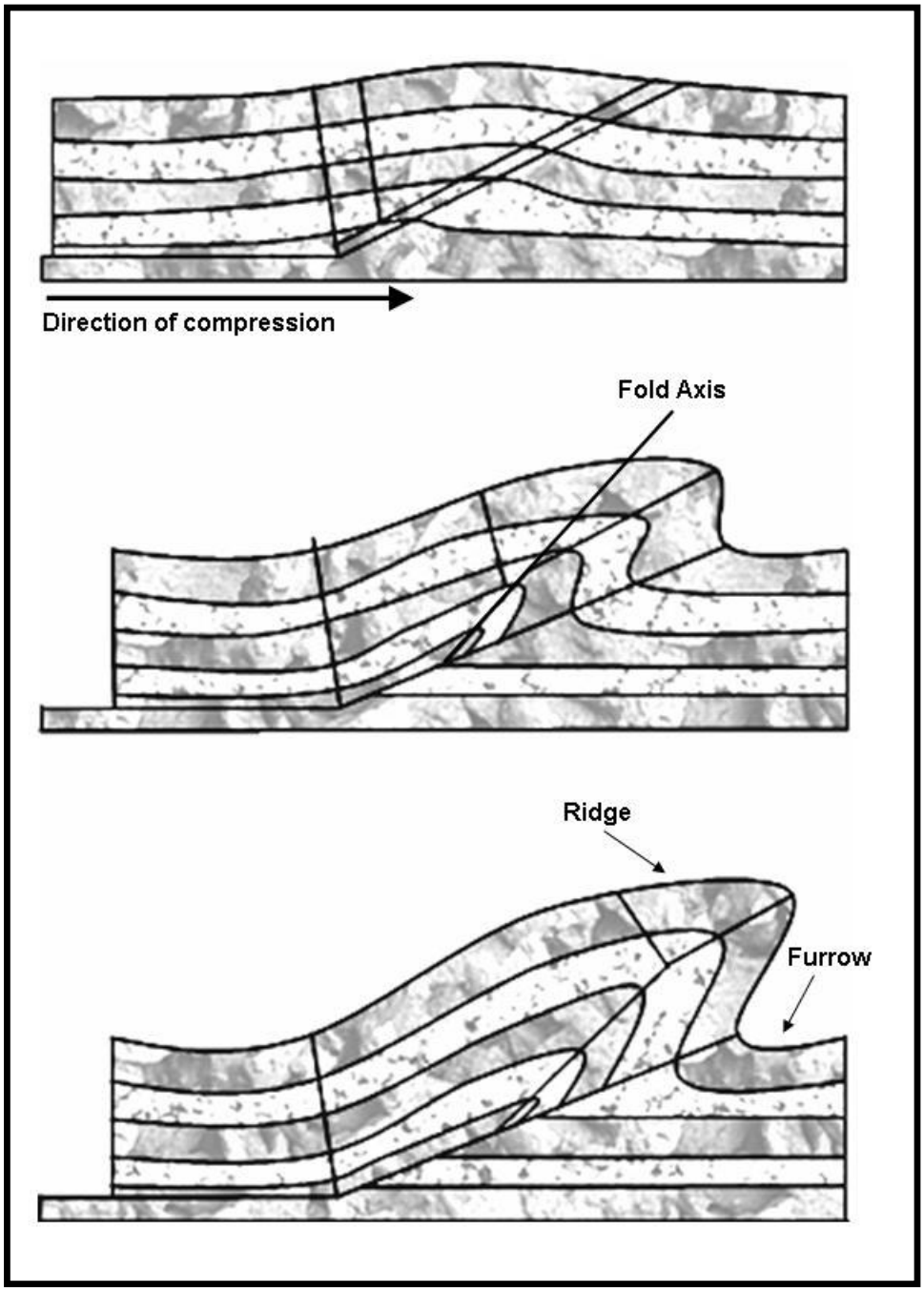

Figure 5. Fault-propogation folding diagram. (Modified after Pollard 2005).

METHODS

Various techniques involving surface morphology mapping, global positioning system (GPS), electromagnetics (EM), and ground penetrating radar (GPR) were used to fulfill the objectives of this study. In earlier work, Zurawek (2002) studied the interior of a relict rock glacier by digging a trench between 2-5 m depth in the lobe of a large debris body on the eastern slope of Mt Sleza, southwest Poland. For this study, non-invasive techniques are preferred because of environmental issues, therefore GPR and EM were used. Drilling or boring tests were not viable because of financial limitations. These tests are also not desirable because of their invasiveness. As a result of the previous excavation on Mount Mestas, a 100 m long and 15 m deep trench was excavated (Johnson, 1967), providing a view of the actual cross-section of the rock glacier without further disturbing the landform. A panoramic photograph of the trench was taken to show the structural cross-section (Figure 6). The trench trends from north to south, so the south end is to the left, and the north end is to the right, as indicated in Figure 6. Ground penetrating radar (GPR) was used as a tool to view the interior structure of several rock glaciers. However, until the validity of using GPR on rock glaciers is proven, all research is based on theoretical concepts of EM wave propagation. The usefulness and accuracy of using GPR as a tool to map the interior structure of a rock glacier was ground-truthed using the excavated trench and the corresponding GPR profiles.

Lab work and field work have been used to ground-truth the usefulness and accuracy of using GPR as a tool to map the interior structure of a rock glacier. The first objective of this study is to map the surface morphology of the rock glacier on Mount

Mestas, the second objective was to view the internal structure of the rock glacier using GPR with supplemental EM data. The third objective was to interpret the panoramic photograph of the exposed trench, and the fourth objective was to ground-truth the use of GPR on rock glaciers using a statistical approach.

Figure 6. Panoramic photograph of Mount Mestas trench.

Surface Morphology Mapping

Mapping the surface morphology of the rock glacier on Mount Mestas was accomplished employing lab work using two black-and-white aerial photographs of Mount Mestas and a stereoscope to map the morphology of the rock glacier. A stereoscope was used to view the study area in 3 dimensions, making it easier to interpret the surface or the rock glacier. The aerial photographs were acquired October 3, 1961. A scale of ~ 1:41,380 was calculated at the center of each photo by using a 1:24,000 scale USGS topographic map. While observing the morphology under a stereoscope, the rock glaciers, frost rubble, avalanche chutes, talus, and vegetation were outlined using standard mapping techniques (Prost, 2001). The crest and the summit of Mount Mestas are also shown on the interpreted image. The interpretation of the photograph was ground-truthed in the field.

A GPS was used in the field to plot the location of the GPR profiles on a digital trace of the rock glacier (Figure 7). By using a GPS, geographic coordinates were measured with a resolution of 2m. Figure 7 shows the location of the head, toe, and the ridge and furrow sequence of the rock glacier along with the location of the GPR profile lines.

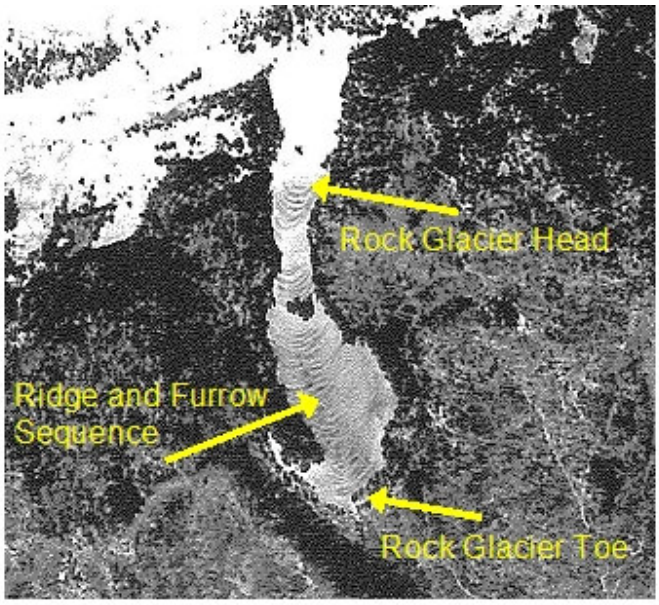

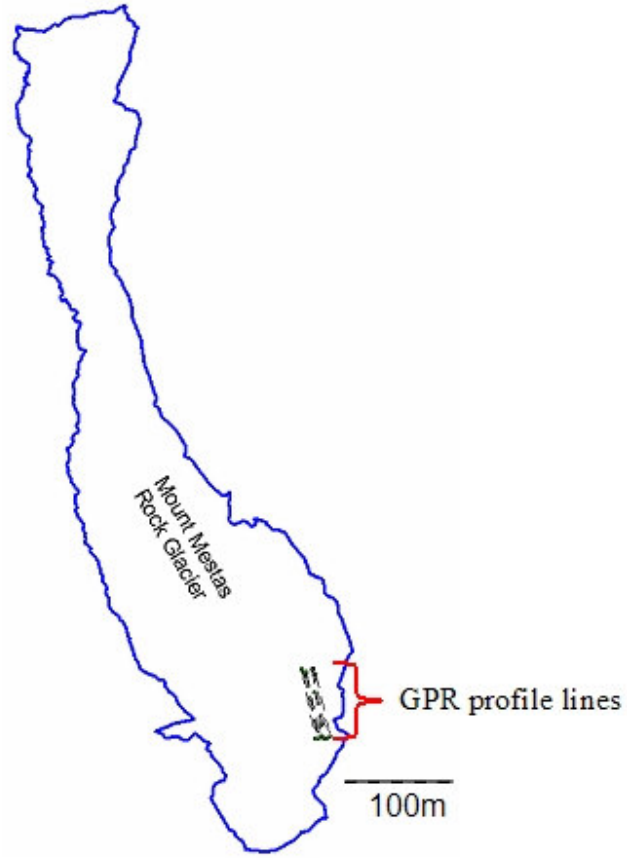

Figure 7. Aerial photograph showing the different parts of the rock glacier along with a geographical outline of the rock glacier showing locations of the GPR profiles.

Construction of Visual Image of Trench

To aid in the comparison of the shear zones and bedding surfaces shown in the rock glacier with the image in the GPR profile, I utilized a panoramic photograph of the trench (Figure 7). The panoramic photograph was prepared using a 6.0 megapixel digital camera mounted on a tripod. Each photograph had an overlap of at least 25% to be certain no gaps were present and to minimize distortion. Using the fabric, or orientation of the clasts, of the rock glacier, I was able to draw in the zones of shear, folding, and bedding surfaces on the image. This step was accomplished in the field and in the lab. In addition, a previous study by Giardino and Vitek (1988) of the fabric of the rock glacier was used to aid in the interpretation of the fabric of the rock glacier.

Electromagnetic Survey

A frequency domain EM34 by Geonics Ltd™ was used to measure the conductivity of the rock glacier, measured in millisiemens per meter. Table 1 shows examples of conductive properties of various geologic materials. These values may differ from *in situ* values, so they will be used only as guidelines for interpretation.

An electromagnetic survey involves the measurement of electric or magnetic field components induced in the subsurface by a primary field, produced from a transient or artificial alternating current source (Figure 8). An alternating magnetic field is established by passing an alternating current through a coil (I_P). The field is measured with a receiver consisting of a sensitive electronic amplifier and meter. The frequency of the alternating current is chosen such that an insignificant eddy current field (I_S) is induced in the ground if it has moderate electrical conductivity. If the source and receiver are brought near a more conductive zone, stronger eddy currents may be caused

to circulate within it and a significant secondary magnetic field (S) will be created. Close to the conductor, this secondary field may be compared in magnitude to the primary field (P), in which case it can be detected by the receiver.

Table 1. Examples of conductive properties of some common materials (Modified after Neal 2004).

Medium	Relative dielectric permittivity (ε_r)	Conductivity (mS/m)
Air	1	0
Fresh Water	80	0.5
Glacial Ice	3.5	0.01
Permafrost	4-5	0.1-1
Unsaturated Sand	2.55-7.5	0.01
Saturated Sand	20-31.6	0.1-1
Unsaturated Sand and Gravel	3.5-6.5	0.007-0.06
Saturated Sand and Gravel	15.5-17.5	0.7-9
Bedrock	4-6	10^{-5}

A conductivity survey is helpful in correlating other types of geophysical surveys. The study area on Mount Mestas is located in a remote location, approximately 14.2 km (8.8 mi) from the nearest town. Therefore, cultural electromagnetic noise should not pose a problem. The EM34 was used to measure the conductivity of underlying material, possibly detecting ice, running water, or bedrock. Both vertical and horizontal dipole excitation were employed, with a 20 m separation. Transverse profiles were made at the 30 m tie line (the figure on page 29).

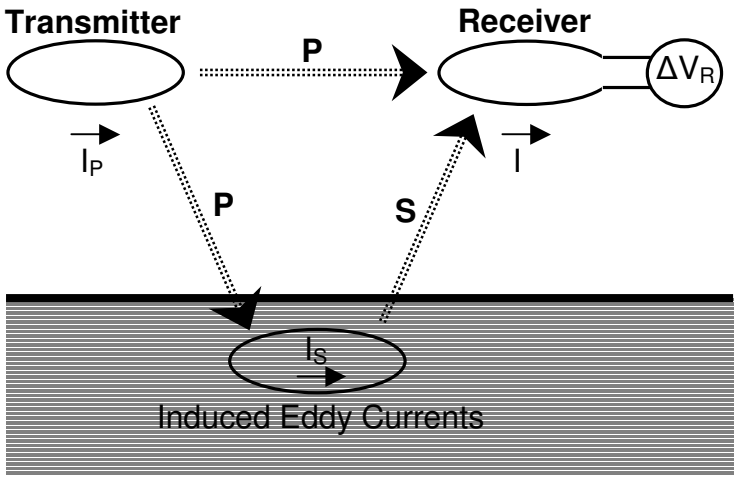

Figure 8. Electromagnetic induction prospecting system. Modified after Sharma (1997).

Ground Penetrating Radar

The PulseEKKO^{TM} 100A radar system from Sensors & Software, INC (Figure 9) was used in perpendicular broadside reflection mode with a constant source-receiver offset to image the subsurface and attempt to match what is seen in the data with what is present in the man-made trench. GPR is state of the art equipment which allows penetration of the surface with electromagnetic waves from a transmitting antenna. As the electromagnetic energy is reflected and refracted off underground discontinuities, a portion of the energy is reflected back to the surface and measured by a receiving antenna (Figures 9 and 10). The material properties that control the behavior of the electromagnetic energy are dielectric permittivity (ε), electrical conductivity (σ), and magnetic permeability (μ). Reflection events can occur from various subsurface

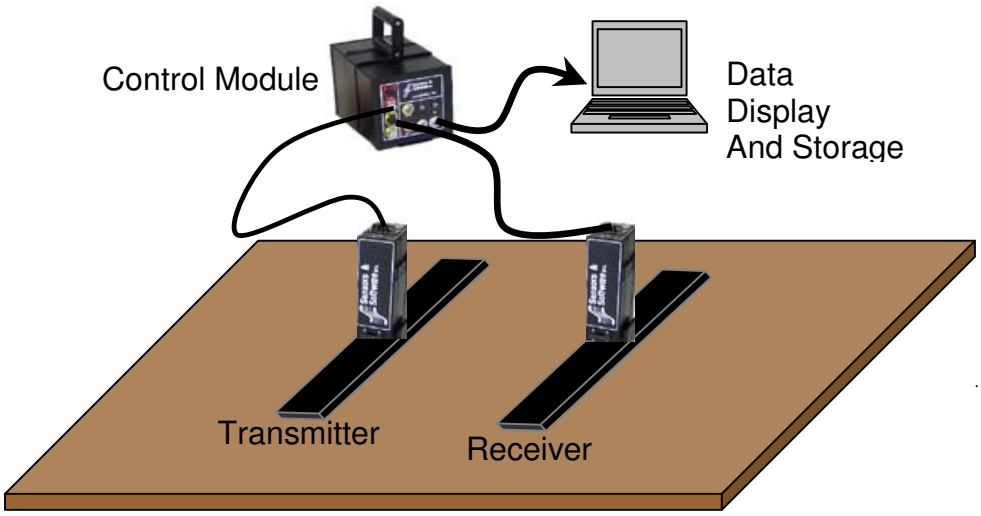

Figure 9. PulseEKKO™ 100A radar system from Sensors & Software, INC.

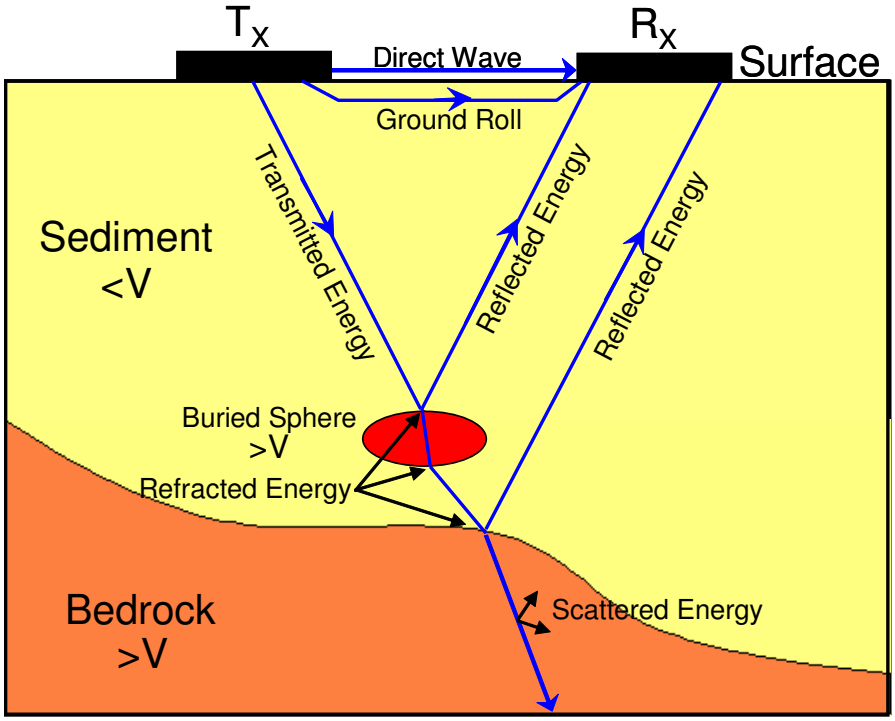

Figure 10. Diagram of the GPR process showing ray paths of transmitted, reflected, and refracted energy. The transmitting and receiving antenna are labeled T_X and R_X respectively. Modified after (Benedict, 1973; Degenhardt et al., 2005).

discontinuities including changes in porosity, changes in sediment grain shape and type, changes in fluid amounts and type, changes in grain orientation, and changes in grain packing. Therefore, geologic features such as sedimentary structures, lithological boundaries, and a water table should be observable with GPR. The two-way radar travel times, from the transmitter antenna to subsurface reflector then back up to the receiver antenna, are then measured and stored digitally on a computer.

A common midpoint (CMP) survey was employed using both 25 MHz and 50 MHz to estimate the radar velocity of the rock glacier medium. This velocity was used for depth conversion and processing of the raw GPR data. A CMP survey is performed with the transmitting and receiving antennas being parallel to each other and perpendicular to the survey direction. Then, by moving each antenna apart successively at increments of 0.5 m for 25 MHz and 0.25 m for 50 MHz, and taking as many readings as necessary to minimize errors associated with dip variations, I was able to obtain an estimate of the underlying media (Figure 11). This was accomplished using the following equation:

$$v_1 = \sqrt{\left[\left(x_2^2 - x_1^2\right) / \left(t_{x2}^2 - t_{x1}^2\right)\right]} \qquad (2)$$

where t_{x1} and t_{x2} are the two-way travel times to the reflection event at antenna separations x_1 and x_2, respectively (Neal, 2004). Thus, the vertical resolution can be obtained by calculating the wavelength (λ), which is governed by frequency and velocity:

$$\lambda = \frac{v_1}{f} \qquad (3)$$

where v_1 *is* a velocity estimate of the underlying media and *f* is the antenna frequency. The maximum resolution achievable may not be better than $\lambda / 4$ (Sharma, 1997). Therefore, I gained better resolution with higher frequency antennas.

The radar wave velocity is related to the relative permittivity (ε_r) by the following equation:

$$v = \frac{c}{\sqrt{(\mu_r \varepsilon_r)}} \qquad (4)$$

where *c* is the speed of light ($3X10^8$ m/s), $\mu_r = \left(\frac{\mu}{\mu_0}\right)$ is the magnetic permeability of the medium, and $\varepsilon_r = \left(\frac{\varepsilon}{\varepsilon_0}\right)$ is the relative permittivity of the medium. For most geologic media $\mu_r = 1$, except for highly magnetic rocks. This makes ε_r the controlling factor of radar velocity.

Horizontal resolution is a function of the step size used when collecting the radar data. The objective in selecting a step size is to sample the subsurface adequately so that geologic structures are well represented in the final radar image. Sensors and Software recommends step sizes for the different size antennas (PulseEKKO, 1996). For higher frequency antennas, a smaller step size is recommended.

The next step was to obtain GPR reflection surveys in a grid fashion with 50 MHz antennas, including nine lines parallel to the trench and three perpendicular tie lines to develop a continuous three-dimensional model of the rock glacier. This was conducted using the common offset (COF) technique. The profiles were shot one trace at a time with a constant transmitter-receiver offset (Figure 12). Nine longitudinal profiles, with a line length of 60 m and station spacing 2 m apart, were collected parallel with the trench (Figure 13). The first profile was parallel to the trench and as close and as possible preventing antenna overhang. The first reading closest to the head of the rock glacier (N) was treated as location zero. Therefore, the GPR readings were taken from high to low elevations or from North to South. Three tie lines were implemented at 1 m, 30 m, and 59 m from the zero location. Antenna frequencies of 25, 50, and 100 MHz were used with step sizes and offsets of 1.0 m, 0.5 m, and 0.25 m, respectively. The profiles were stacked 64 times at a rate of 800 s^{-1}.

The GPR data were processed using Win_EKKO Pro® by Sensors & Software, INC™. After processing the data, the shear planes, bedding surfaces, and the bedrock interface were interpreted.

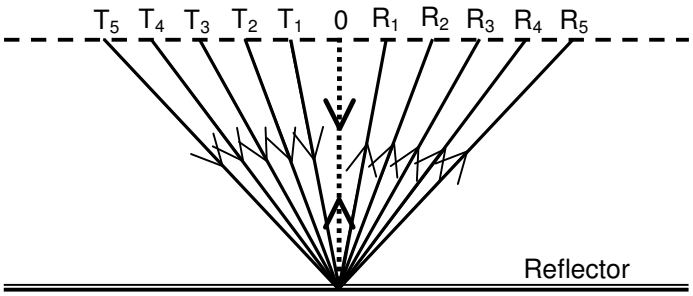

Figure 11. Common midpoint survey showing ray paths of reflections from the Transmitter (T_X) to the Receiver (R_X).

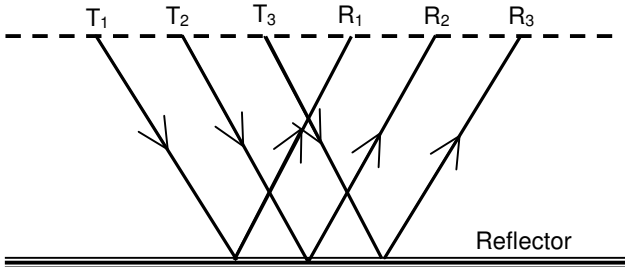

Figure 12**.** Common offset reflection technique showing ray paths of reflections from the Transmitter (T_X) to the Receiver (R_X).

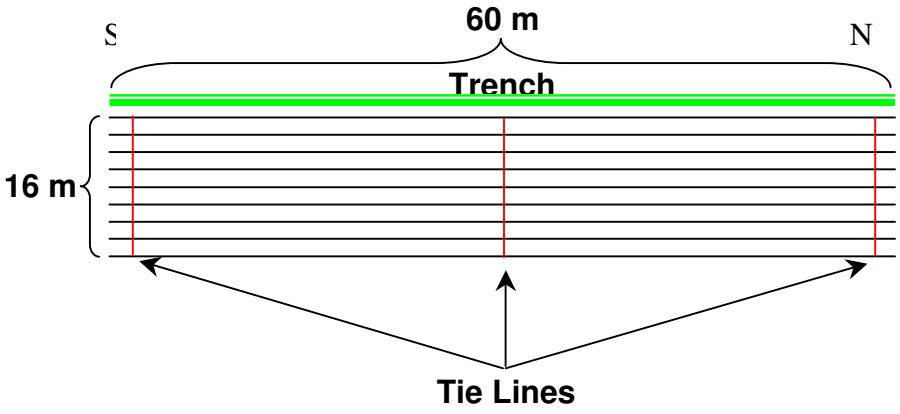

Figure 13. Profile layout.

Ground-Truth the Use of GPR

A statistical comparison between GPR data and the actual profile was conducted to ground-truth the use of GPR to construct views of the internal structure of rock glaciers. Three series of statistical t-tests were run. The first series of tests compared the trench and GPR profiles in 25 ns increments, dividing them into twelve sections. The second series of tests divided the profiles into 25 ns increments, creating six vertical sections. The third series of tests divided them into 100 ns increments, creating three vertical sections. Next, the number of structures and/or surfaces detectable in both were determined. For the 25 ns divisions, structures greater than 2 m were counted, for the 50 ns divisions, structures greater than 5 m were counted, and for the 100 ns divisions, structures greater than 10 m were counted. The statistical t-test was used to determine whether the comparisons between the trench and profiles are statistically significant. The t-value is essentially a signal to noise ratio (Equations 5, 6, and 7). Nine t-tests were run; each using the trench as the control group (X_C) and the GPR profile as the group being tested (X_T). For this study, the control group was the standard by which the experimental observations were evaluated:

$$\frac{Signal}{Noise} = \frac{\overline{X}_T - \overline{X}_C}{SE(\overline{X}_T - \overline{X}_C)} \tag{5}$$

$$SE(\overline{X}_T - \overline{X}_C) = \sqrt{\frac{\mathrm{var}_T}{n_T} + \frac{\mathrm{var}_C}{n_C}} \tag{6}$$

The numerator of equation 5 is the difference of the means between the two groups. The denominator is a measure of variability between the two groups, or the standard error of the difference. Equation 6 shows how to calculate the standard error of the difference. The final formula for the t-test is shown in equation 7.

$$t = \frac{\overline{X}_T - \overline{X}_C}{\sqrt{\frac{\text{var}_T}{n_T} + \frac{\text{var}_C}{n_C}}} \qquad (7)$$

For this study, the null hypothesis (H_0) is $\mu_1 = \mu_2$, where μ_1 is the photograph interpretation and μ_2 is the GPR profile interpretation. After the t-value was calculated, the P-value was established from a t-table. Using a significance level of $\alpha = 0.05$, the P-value indicated whether the results are statistically significant at the 5% level. If the P-value is small compared to the significance level, one can reject the null hypothesis.

Various techniques including surface morphology mapping, global positioning system (GPS), electromagnetics (EM), and ground penetrating radar (GPR) were used for this study. Utilization of these four objectives provided the knowledge and resources to arrive at the goal of ground-truthing GPR as a useful tool to view the interior structure of rock glaciers.

RESULTS AND ANALYSIS

Techniques such as surface morphology mapping, global positioning system (GPS), electromagnetics (EM), and ground penetrating radar (GPR) were used in this study. Both lab work and field work were employed to ground-truth the usefulness and accuracy of utilizing GPR as a tool to map the interior structure of a rock glacier.

Surface Morphology Mapping

Surface morphology mapping of the Mount Mestas area was helpful in gaining a better understanding of the study area prior to the field study. Features including the summit, crest, frost rubble, avalanche chutes, rock glaciers, and talus and vegetation were mapped (Figure 14). The summit is the highest elevation attainable on a mountain, the crest is the top line or ridge of the mountain, and avalanche chutes are the preferred paths taken by debris. Talus is referred to as the rock debris that accumulates at the base of a slope which was formed by erosion of material from higher elevations. Frost rubble has been defined as:

> …a deposit of angular blocky or irregular shaped rock fragments of pebble or larger size that contains little or no matrix, has no cliff or prominent ledge at its head, and is primarily the product of frost action (1962:19) (Richmond, 1962).

A GPS was also used to outline the rock glacier containing the study area (Figure 7). The length and width of the rock glacier is approximately 200 m and 800 m, respectively. The rock glacier covers an area of ~ 160,000 m^2.

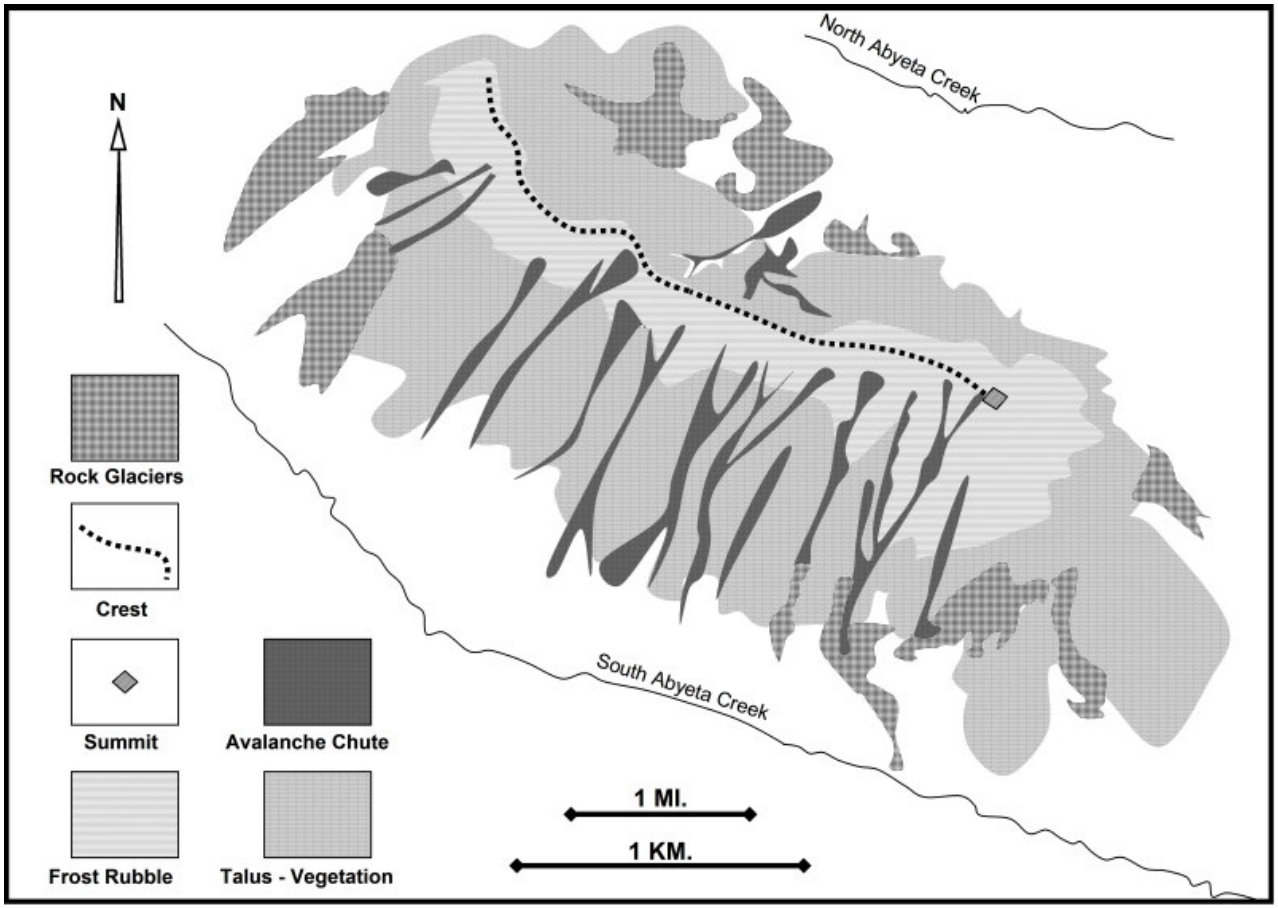

Figure 14. Local geomorphology map of the area.

With prior knowledge of the study area, researchers are better able to understand the forces acting on the system. Mount Mestas has been weathering for millions of years, since the Tertiary period. This pluton, composed of homogeneous felsite, fractures into platy slabs (Giardino and Vitek, 1988) that were created at higher elevations and descended towards the base. Talus takes alternate downward routes, such as avalanche chutes or rock glaciers, to arrive at its present location.

Construction of Visual Image of Trench

In Giardino and Vitek's (1988) paper, fabric zones in the vertical excavated trench on Mount Mestas that had preferential clast orientation were delineated. Their paper shows an average fabric orientation dip being 13.8^0 from perpendicular of the sample population. Clasts dominated the internal fabric of this rock glacier, with the majority being between 10 and 70 cm (Giardino and Vitek, 1988).

A panoramic photograph was used for this study to interpret the vertical cross section of the excavated trench. The panoramic image was first printed on plotter paper that measured 36 inches high by 48 inches wide. A 40 m long section of the trench was chosen for interpretation because of a satisfactory visual appearance, such as sparse vegetation and minor amounts of loose, or not *in situ*, clasts. By viewing the fabric, or orientation of the clasts, the zones of shear, folding, and bedding surfaces were drawn in red (Figure 15). The blue line represents the surface of the rock glacier or the top of the trench.

Figure 15. Panoramic photograph of the trench with the interpreted image.

Electromagnetic Survey

An electromagnetic surveying technique was utilized to determine whether a presence of water or ice could be detected. Time has been spent on a known active rock glacier in Yankee Boy basin near Telluride, CO, during the summer months. Running water could be heard flowing beneath the surface, and ice was visible through the rock's interstices. However, the Mount Mestas rock glacier does not exhibit these characteristics. The evening before the EM technique was conducted on Mount Mestas, a rain storm passed through; however, a noticeable flow of water was not apparent, and ice was not visible. Because moisture content greatly influences conductivity, EM readings may exhibit interference from the runoff. Nonetheless, the survey was conducted.

The survey was begun using a 10 m coil separation with vertical inductance (horizontal coil planes), allowing an effective exploration depth of approximately 7.5 m. The results were null, implying very resistive near-surface material. This is consistent with the near-surface material that is composed of dry fragments of igneous origin (Table

1). The high resistivity of the material will allow deep penetration of the EM signal because it is not being attenuated rapidly. Our second test utilized a 10 m separation with horizontal inductance (vertical coil planes), allowing an effective exploration depth of approximately 15 m. Again the results were null, implying high resistivity near-surface. Our third test was made using 20 m separation and vertical inductance, allowing effective exploration depth of about 20-25 m. Table 2 shows the measured readings, with position 0 being nearest to the trench. Figure 16 shows the measurements in millisiemens m^{-1} plotted against distance in m from the trench. The readings of 2.1-0.45 mS/m are very small, indicating an area of low conductivity around 20-25 m depth. This area may be composed of a layer of fine grained material or permafrost below a zone of aeration. Perching of fresh water with low total dissolved solids (TDS) may also exist on top of the low conductivity layer.

Table 2. EM conductivity measurements achieved with 20 m coil separation and vertical inductance.

Position (m)	mS/m
0	2.1
4	1.75
8	1.35
10	1.1
12	0.8
16	0.45

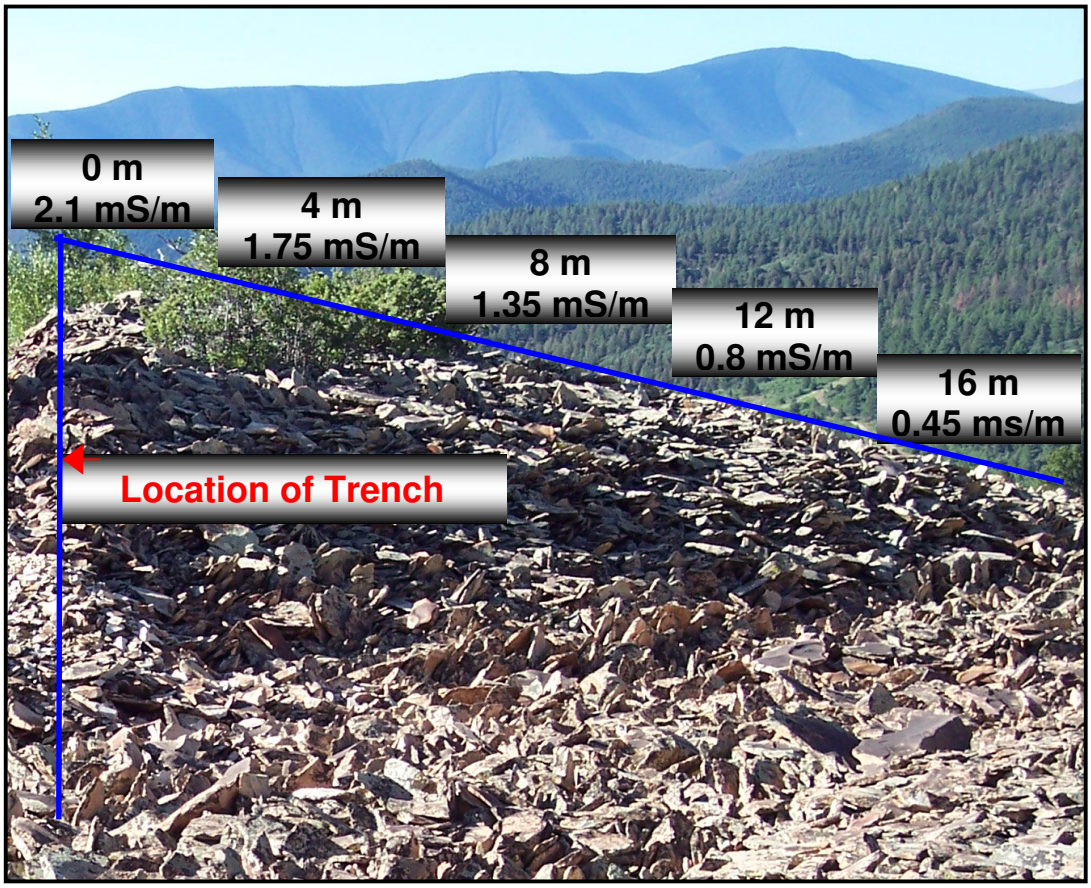

Figure 16. Location and amplitude of EM conductivity readings perpendicular to trench

Ground Penetrating Radar

GPR surveys were conducted following the EM surveys. The survey began with CMP analyses to obtain a radar velocity estimate of the rock glacier medium. Two semblance analyses were conducted parallel to the trench with $f = 25$ and $f = 50$. The results of the CMP surveys are shown in Figure 17. Both surveys yield a best fit velocity value of 0.15 m/ns for the upper 200 ns. Depth estimation was also accomplished using this average velocity, equal to a dielectric permittivity (ε_r) of 4, showing consistency with

permafrost. The 25 MHz CMP analysis shows a low velocity value for the reflection occurring between 200 – 300 ns (15-22.5 m) of 0.065 m/ns, which is absent in the 50 MHz CMP implying that 25's generate deeper penetration. This equates to a relative dielectric permittivity (ε_r) of 21.16, consistent with saturated sand (Neal, 2004).

After a best fit radar velocity on the rock glacier was resolved, a common-offset (COF) survey was conducted. The reflection surveys paralleled the excavated trench from higher to lower elevations. Profiles of 60 m were chosen for the purpose of identifying whether a link could be established between the GPR reflections and the internal structure of the trench. Data were collected within two summers.

GPR surveys were conducted using 25, 50, and 100 MHz antennas. Profiles were obtained with the PulseEKKO^{TM} 100A radar system set up in perpendicular broadside reflection mode, and the profiles were stacked 64 times at a rate of 800 s^{-1}. Using equation 3, the dominant wavelengths were calculated using a velocity of 0.15 m/ns. Wave theory tells us that the best vertical resolution that can be achieved is one-quarter of the dominant wavelength (Sheriff, 1977); therefore, the vertical resolution is 1.5 m for 25 MHz antennas, 0.75 m for 50 MHz antennas, and 0.375 m for 100 MHz antennas. Horizontal resolution is a function of the step size used when collecting the radar data. The objective in selecting a step size is to sample the subsurface adequately so that geologic structures are well represented in the final radar image. Sensors and Software recommends step sizes for the different size antennas (PulseEKKO, 1996). For higher frequency antennas, a smaller step size is recommended. The profile lengths were 60 m long, and step sizes of 1.0 m for $f = 25$, 0.5 m for $f = 50$, and 0.25 m for $f = 100$ were used. The results of the COF surveys are shown in figures 18 through 23.

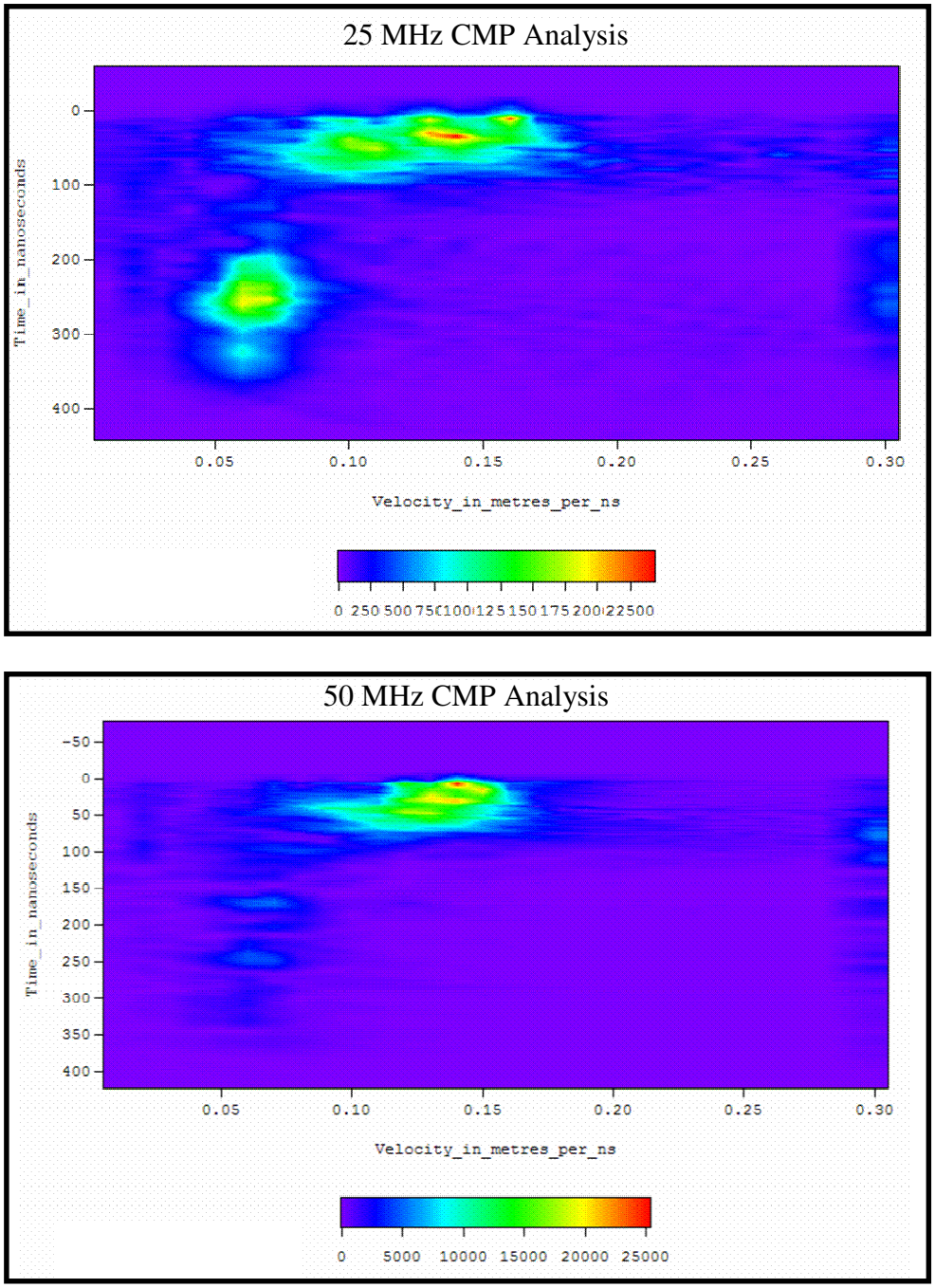

Figure 17. CMP analysis of Mount Mestas rock glacier showing average velocity at 0.15 meters per nanosecond [m/ns].

Processing of the GPR data were accomplished using Win_EKKO Pro® ground penetrating radar software developed by Sensors & Software. Minimal processing was applied to maintain accurate data. The raw 25 MHz data were first processed using a DEWOW filter to reduce the low-frequency 'wow' induced by signal saturation of the receiving antenna. The data were filtered using automatic gain control (AGC) with GMAX = 50. The data were then migrated using the average calculated velocity of 0.15 m/ns as determined by the CMP analysis. Processing of the 50 MHz and 100 MHz profiles were similar to that of the 25 MHz profile, with the exception that they were filtered using GMAX = 150. On all profiles, the horizontal scale is distance in meters, the left vertical scale is two-way travel time in nanoseconds (ns), and the right vertical scale is depth in meters (m). The blue horizontal line represents the base of the trench. The two earliest continuous reflections on each profile symbolize the air wave and ground wave arrivals, respectively. Resolution increases with higher frequencies, as shown in Figures 18, 19, and 20.

Numerous reflections of varying coherency are visible within the profiles. These represent structural and stratigraphic discontinuities within the rock glacier. With the 25 MHz antennas, the theoretical vertical resolution was calculated to be 1.5 m; therefore, any layer visible in the radar profile has a thickness greater than 1.5 m. Noise was created by air and surface waves in the upper 7 m of the 25 MHz profile (Figures 18 and 21). The unprocessed (Figure 18) as well as the processed radar profiles (Figure 21) show coherent reflections from ~75 to ~475 ns. An anticline prevalent in the radar profile at ~35 m corresponds to a surface ridge. A strong continuous reflection between ~275 and ~475 ns corresponds to a contact between the upper zone of aeration and lower

layer of ice-saturated sediment, or permafrost. Two strong onlapping reflections terminate against the contact and dip in a general downslope direction. This is consistent with the fault-propagation theoretical model of ridge and furrow development. Weak reflections occur from 350 ns down to 600 ns (~45 m), which is the lowest detectable limit achieved by the GPR at this frequency. The reflections between 400 ns and 600 ns are lost because of processing. This profile was divided into three zones. The upper zone, from 85 ns to ~275 ns is interpreted as the zone of aeration where most voids are occupied by air. The second zone, from ~275 ns to ~400 ns represents the zone of saturation where voids are filled with water or ice-saturated fine-grained sediment. The lower zone represents layers of unsaturated material.

The 50 MHz antennas have a theoretical vertical resolution of 0.75 m. Therefore, only layers greater than 0.75 m will be detected. The processed 50 MHz is shown in Figure 22. Coherent reflections can be observed from ~75 to ~475 ns in this profile. The two earliest reflections represent air and surface waves, respectively, creating noise in the upper 4 m. The anticline occurring at ~35 m is still evident in this profile as it was in the 25 MHz radar section. Strong coherent reflections are prevalent around ~275 to ~ 475 ns, and are consistent with the 25 MHz section. Ridge and furrow sequences can also be distinguished around 75 ns. The stratification resembles herringbone-cross stratification, with the overlying layers dipping down towards the south and the lower layers dipping down towards the north. These dipping events converge at a strong reflection at around 300 ns. A three layer model can be assumed for this profile as well. An obvious resolution increase is apparent between the 25 MHz and the 50 MHz profiles. A three-

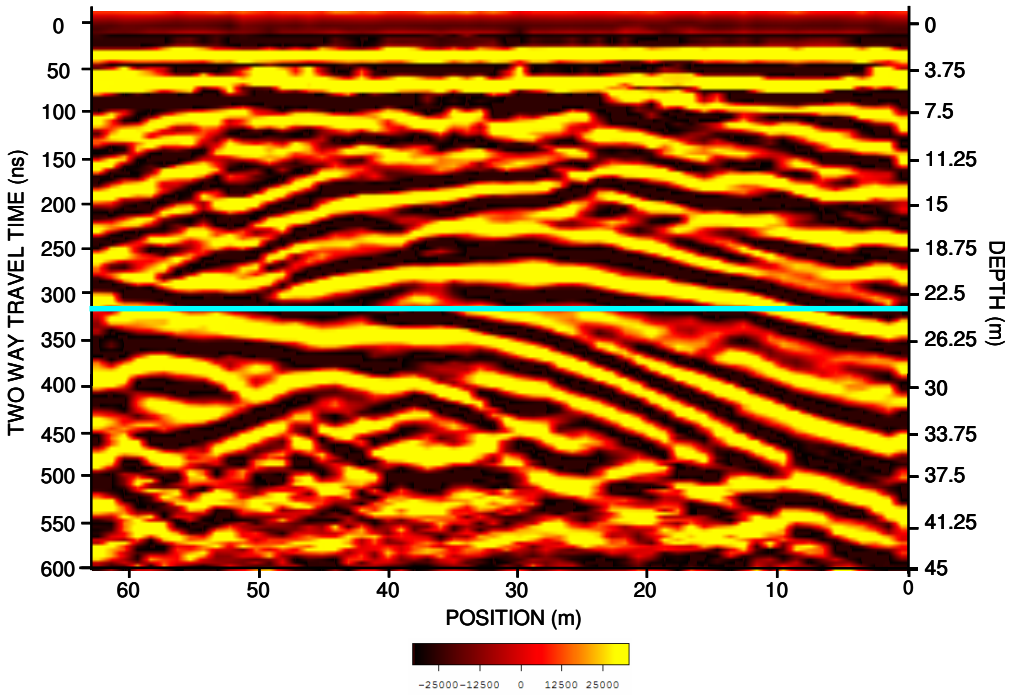

Figure 18. Unprocessed GPR profile using *f*=25 with step size of 1 m.

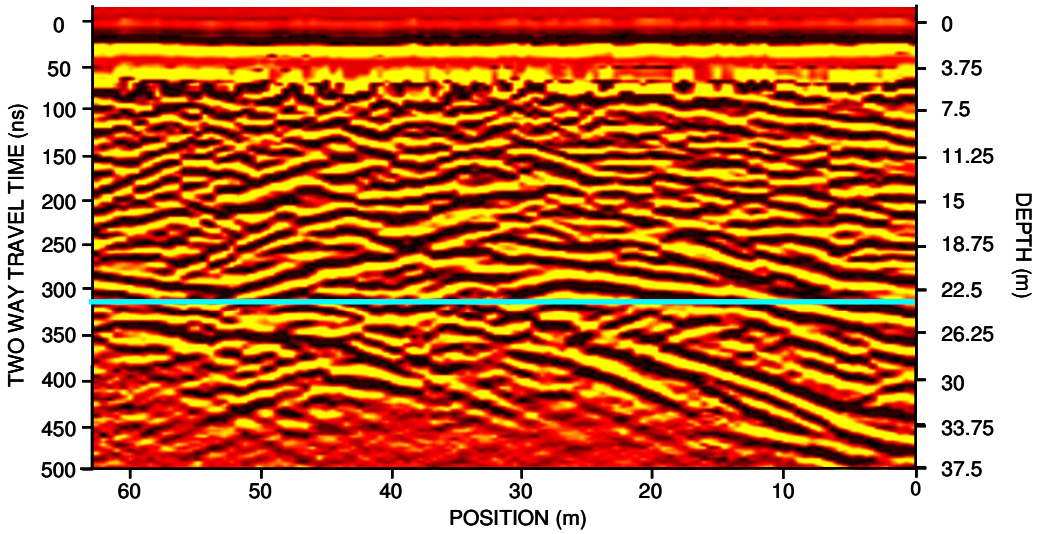

Figure 19. Unprocessed GPR profile using *f*=50 with step size of 0.5 m.

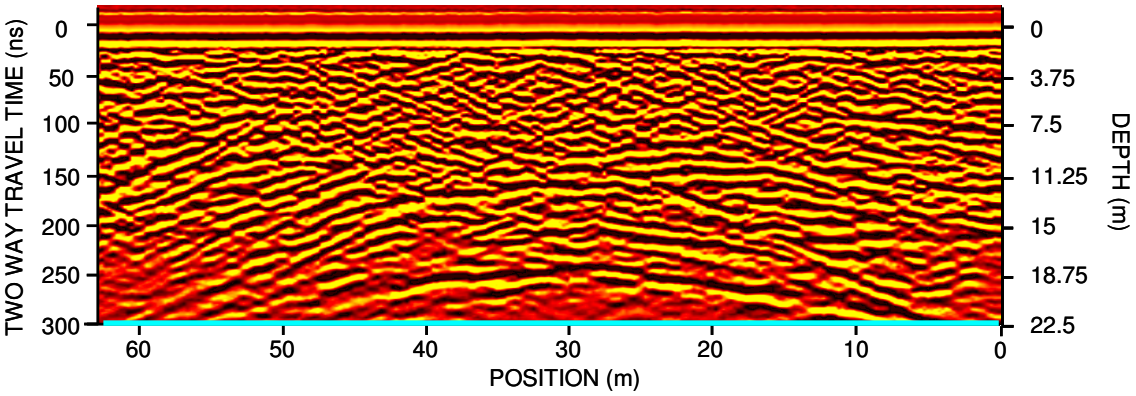

Figure 20. Unprocessed GPR profile using *f*=100 with step size of 0.25 m.

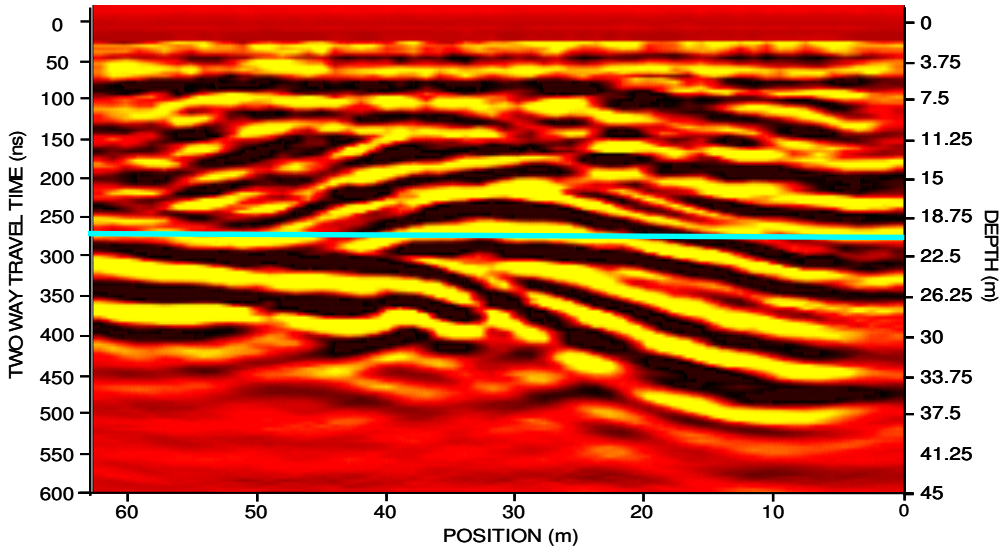

Figure 21. Processed 25 MHz radar profile.

dimensional model was created using 50 MHz profiles because this wavelength depicts continuity of the anomalous layer most accurately. Figure 23 is situated to where the trench is to the right, and the GPR profiles cut into the rock glacier moving left. It shows clearly how the anomalous layer cuts through the entire survey. The dark blue layer representing the anomaly is consistent throughout the center of the profile and is also consistent with the trench's depth of 23 m.

By using 100 MHz antennas, depth of penetration is decreased whereas resolution increases. Air and surface waves created noise in the upper 2 m. The processed 100 MHz radar profile is shown in Figure 24. With a calculated theoretical vertical resolution of 0.375 m, individual clasts are evident. Coherent reflections can be detected from ~25 to ~300 ns in the 100 MHz profile. Radar antennas radiate and receive electromagnetic energy in a complex 3-dimensional cone; therefore, the unprocessed and unmigrated radar reflection profile shows a complex sequence of cross-cutting diffractions or hyperbolas (Figure 20). These have resulted from clasts that are large (>0.375 m) with respect to radar wavelength and act as individual reflector points. Diffractions can obscure primary reflections. The processed data were migrated and the diffractions were collapsed to reveal a more realistic image of subsurface reflections. Many structural features such as onlapping and downlapping reflections are discernable in the 100 MHz profile that were not apparent in the 25 or 50 MHz profiles. A portion of the strong reflector seen in the 25 and 50 MHz profiles is distinguishable in the 100 MHz profile at 275 ns. The anticline noticed at ~35 m is still prevalent.

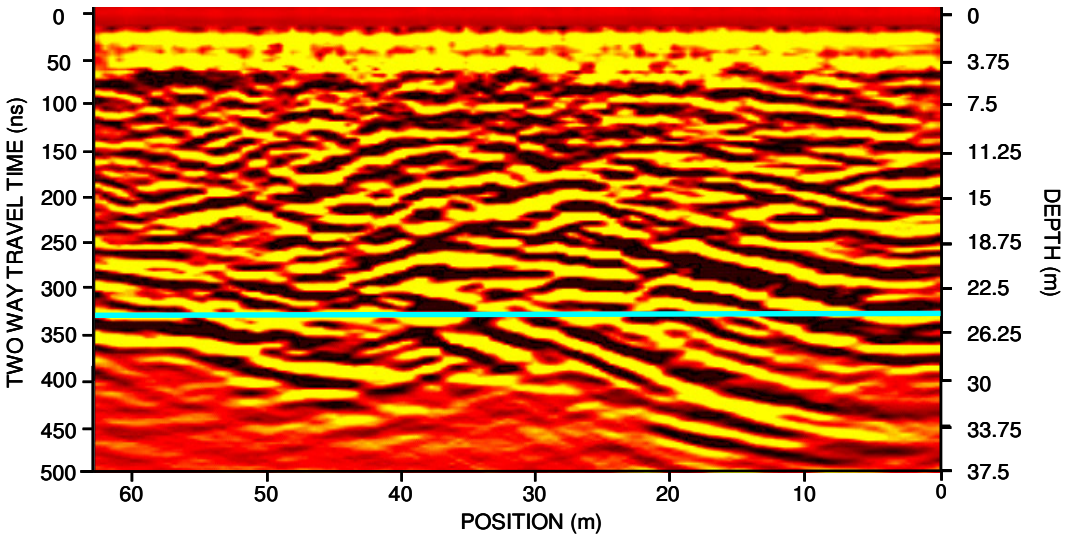

Figure 22. Processed 50 MHz radar profile.

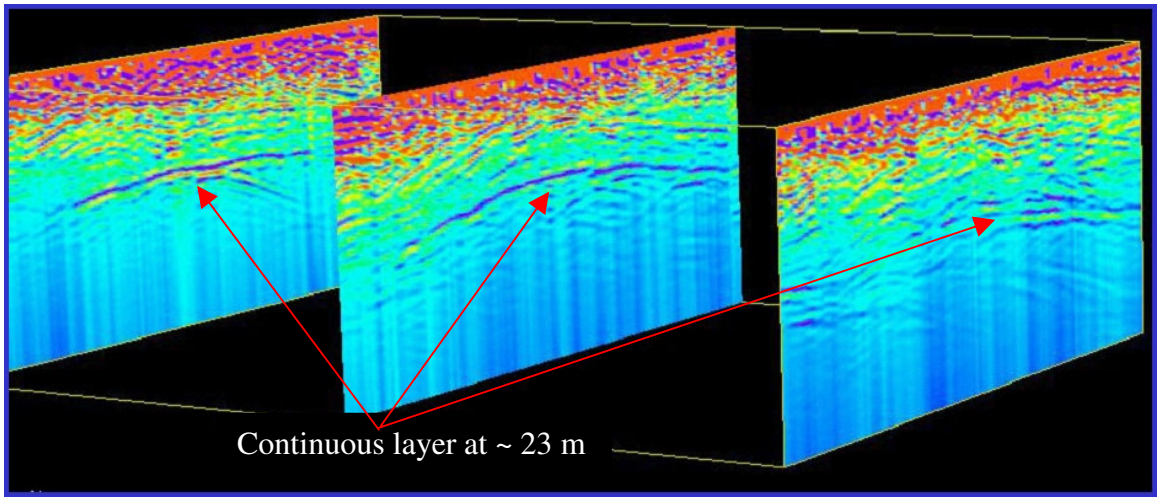

Figure 23. 50 MHz GPR profiles showing continuity of anomalous layer.

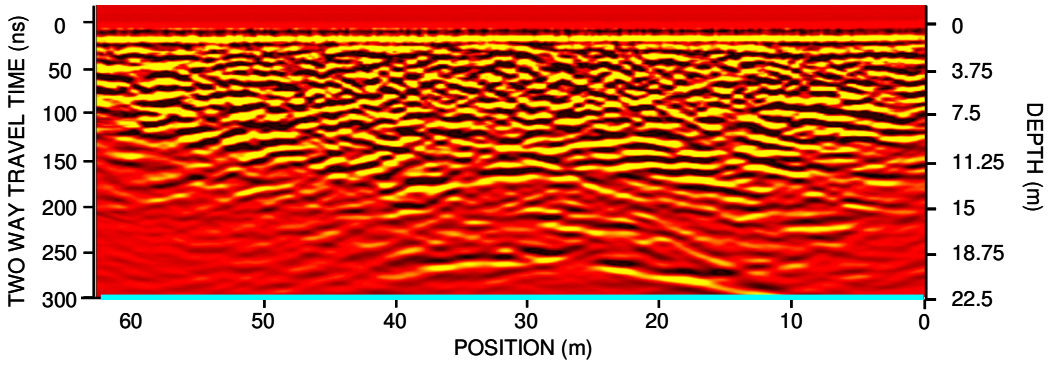

Figure 24. Processed 100 MHz radar profile.

Over the last fourty years, debris has worked free from the vertical scarps created by the excavation and have fallen into the trench. As a result, the base of the trench has been covered by sediment and air-borne particles; consequently, we were unable to obtain samples of the anomaly. Nonetheless, the depth of the anomaly located by each tool is identical to the approximate depth of the trench. The EM34 by Geonics Ltd™ reveals an area of low conductivity at ~20-25 m depth. The CMP analysis obtained with 25 MHz antennas indicates a low velocity zone at 22.5 m. Each GPR profile, including the 25 MHz, 50 MHz, and the 100 MHz profile show a strong reflection at the same depth. This leads me to believe that when the Colorado Highway Department was digging the trench, they reached the top of an ice layer, so they halted the excavation.

Ground-Truth the Use of GPR

To compare the trench cross-sectional profile with the GPR data, structural interpretation is necessary. The fabric, zones of shear, folding, and bedding surfaces are outlined in red on a panoramic photograph of the trench (Figure 16). The horizontal

positions used for interpretation range from 12 m to 50 m due to a satisfactory visual appearance, such as sparse vegetation and minor amounts of loose, or not in situ, clasts. The vertical extent ranges from 0 ns (0 m) to 306 ns (23 m). The GPR profiles were also examined. GPR data were interpreted after processing was applied. Primary reflections were traced and are inferred as sedimentary structures, lithological boundaries, and saturation contrasts. Figure 25 shows the section being compared.

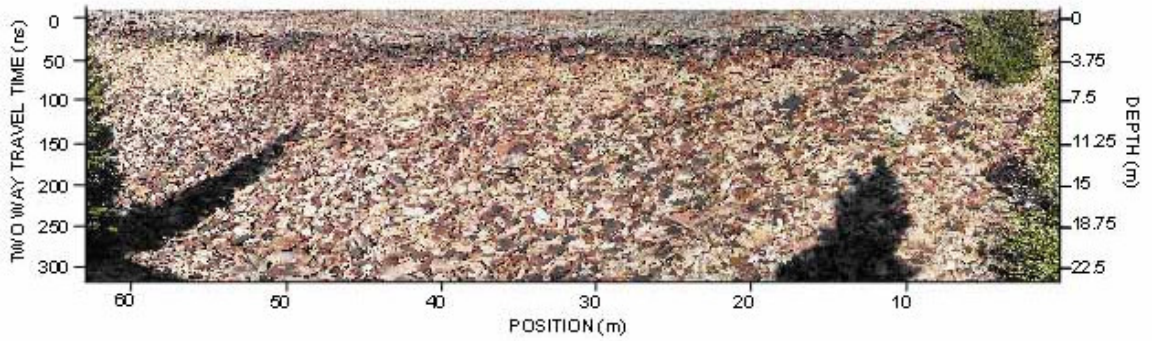

Figure 25. Trench section being compared with GPR profiles.

Figure 26 shows the trench interpretation (red lines) blanketing the interpreted 25 MHz GPR profile (black lines). The upper 7 m of the GPR profile were unable to be interpreted because of noise produced from the air and ground waves. The horizontal red line indicates the base of the trench. The individual traces of fabric from the panoramic photo do not match exactly with the GPR profile, perhaps because the limit of vertical resolution allowed by the 25 MHz antenna. Above ~300 ns, the GPR reflections show a

general trend dipping towards the left (south), agreeing with the dipping lithology interpreted in the panoramic photo.

The 50 MHz profile was interpreted similar to the 25 MHz profile; however, with the resolution enhanced two-fold. Vertical resolution for this GPR profile is 0.75 m, therefore the receiver will receive radar signals from layers with thicknesses greater than 0.75 m. Figure 27 shows the trench interpretation (red lines) blanketing the interpreted 50 MHz GPR profile (black lines). The air and ground waves mask only the upper ~4.25 m of the GPR profile. The preferred orientation of the upper 300 ns is comparable to the previous profile with a general trend dipping in the southerly direction. A small anticlinal fold is evident in both the trench and GPR interpretation at ~ 100 ns and 47 m.

Figure 28 shows the trench interpretation (red lines) blanketing the interpreted 100 MHz GPR profile (black lines). The 100 MHz radar antennas detected features greater than 0.375 m in thickness within the rock glacier. The clasts range from 10 to 70 cm in length, therefore individual point sources of radar reflections were received, causing diffraction hyperbolas to appear within the data. However, after migration was applied, the diffractions were collapsed, revealing several individual reflections less than 2 m in magnitude. These small reflections may correspond to individual clasts within the profile. The GPR data show a clear trend of dipping lithology toward the south, which along the northern portion of the data, the trend dips toward the north at lower angles. The center of the profile exhibits anticlinal features, giving the data an overall hyperbolic appearance.

Rock Glacier Morphology

The rock glacier flows in a fixed line until an inflection point ~ 350 m from the head, at which point it takes a 20^{o} bend toward the East. The inflection point is caused by a change in topography, where the vertical relief is greater to the east. The vertical relief decreases past the inflection point and causes the rock glacier to spread out laterally. As the rock glacier spreads out, it blankets the bedrock morphology, and any irregularities on the bedrock surface will translate onto the surface of the rock glacier. A mound is apparent at the study location, which is possibly because of a knob irregularity of the bedrock.

The ridges and furrows on the rock glacier are caused by variable flow velocities with depth and form perpendicular to the direction of flow. Surface flow velocities are greater at the center of the rock glacier, and decrease with increasing distance toward the exterior. This is shown buy the hyperbolic shape of the ridge and furrow sequence.

The internal structure of the rock glacier contained in the GPR profiles possesses one large-scale thrust fault that was formed by the anomaly occurring between ~ 200 – 450 ns, also known as zone 2 (Figure 29). This thrust fault does not alter the surface morphology. A decollement surface, or a surface that acts as a gliding plane, exists between zones 1 and 2. Small scale thrust-related faulting is occurring between 0 and 200 ns. There seems to be no order of events, but instead random series consisting of complex series of duplex structures, fault-bend folding, and fault-propagation folding.

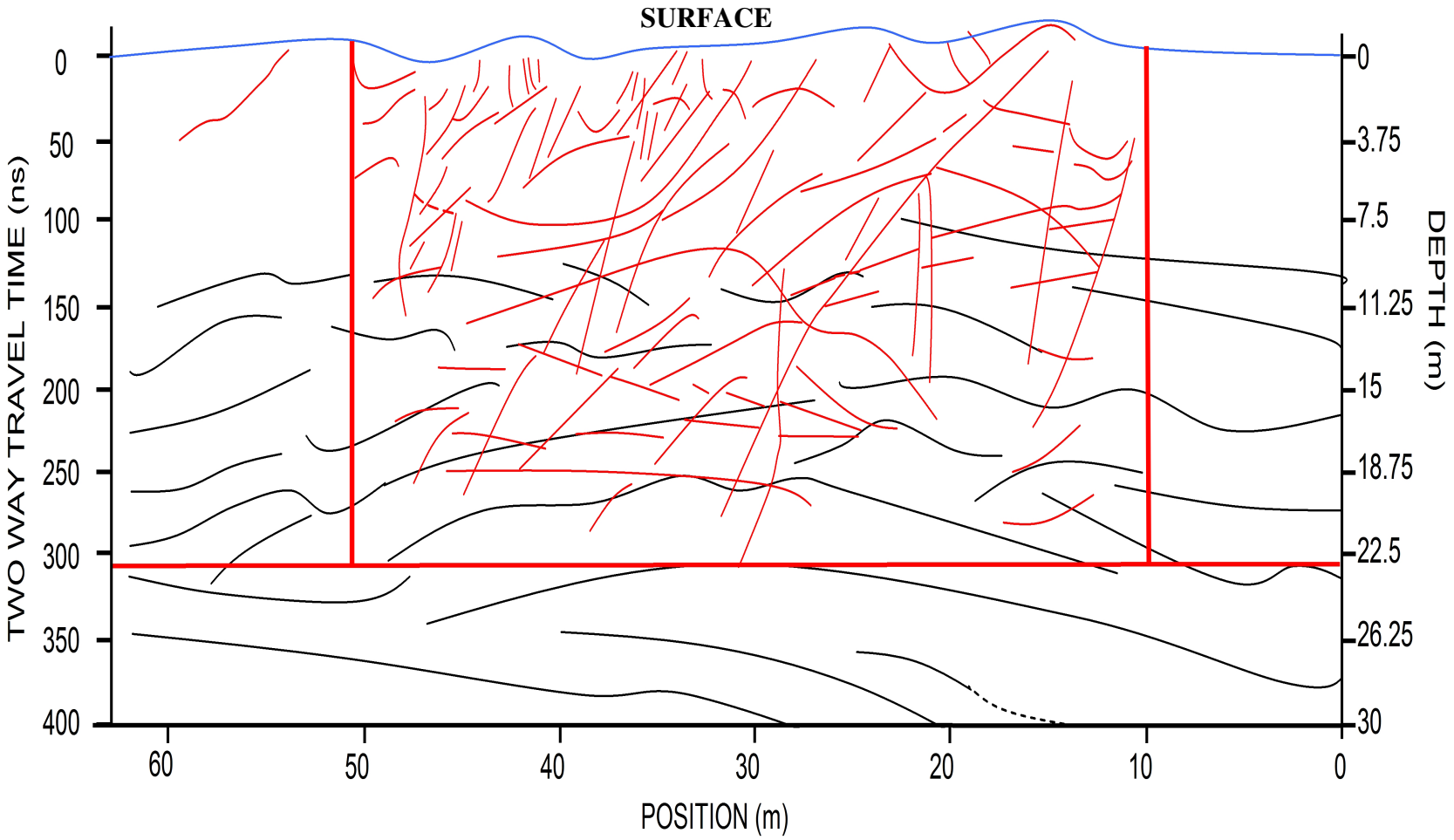

Figure 26. Interpreted 25 MHz GPR profile overlain by interpreted trench cross-section.

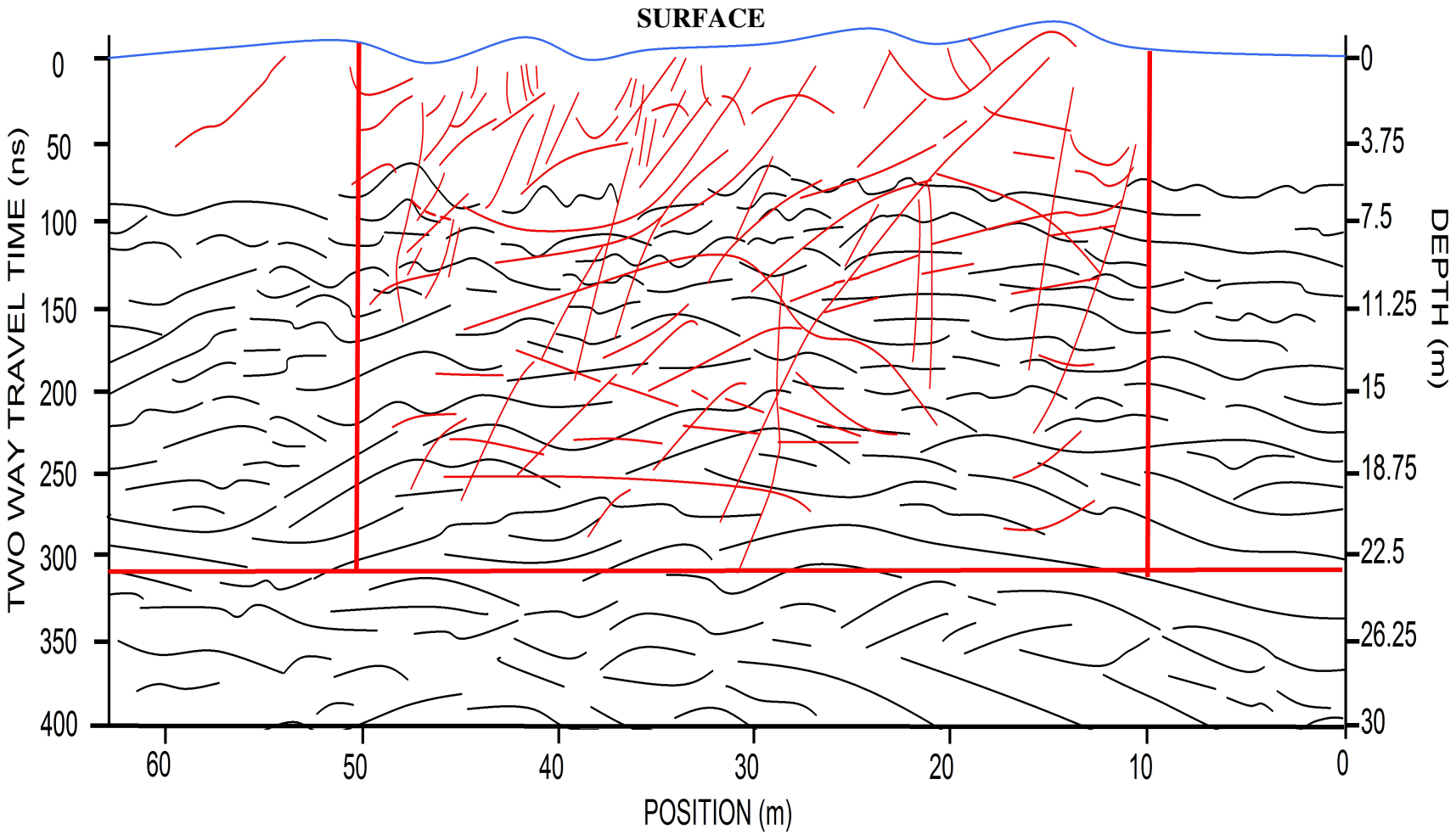

Figure 27. Interpreted 50 MHz GPR profile overlain by interpreted trench cross-section.

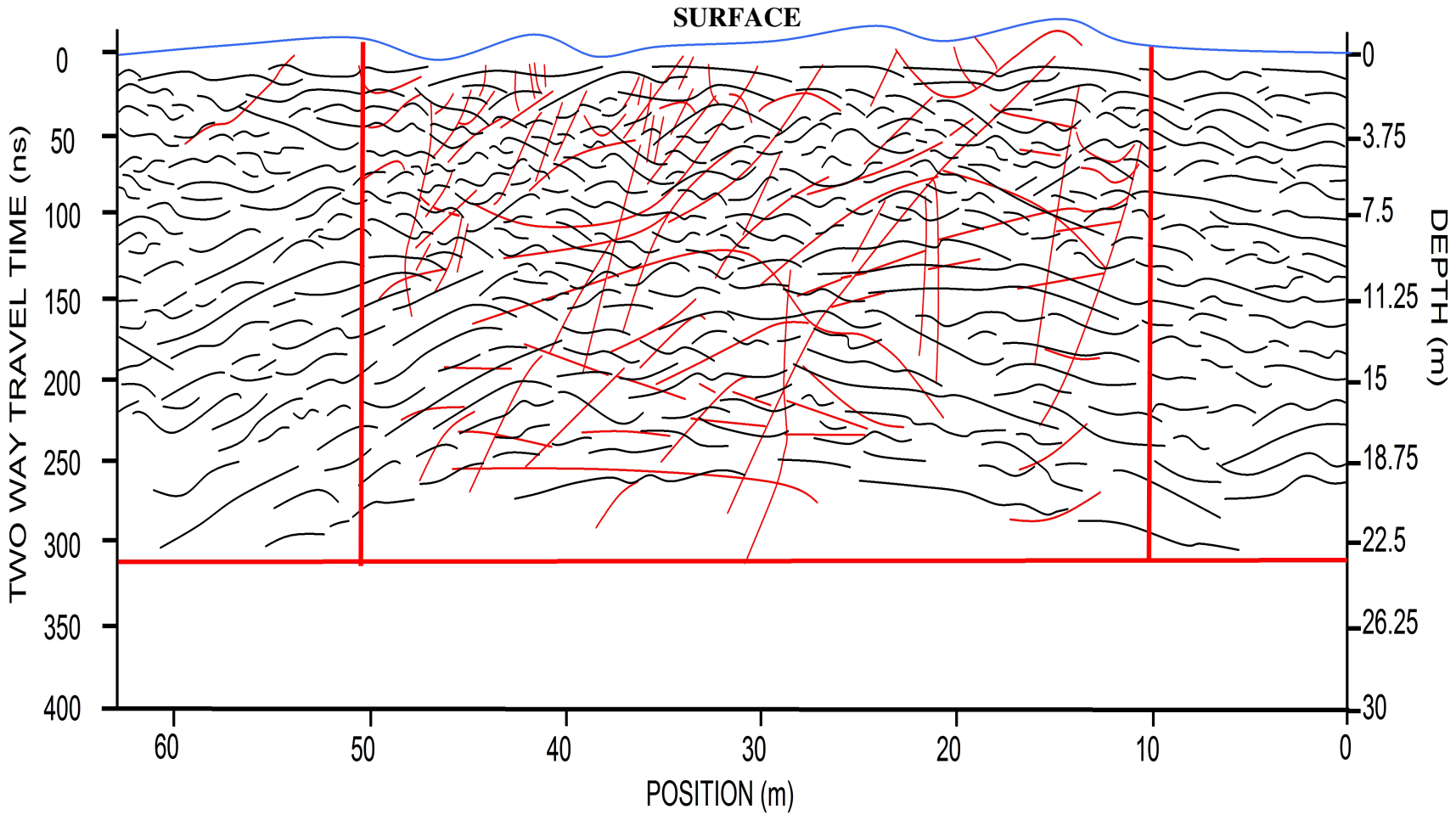

Figure 28. Interpreted 100 MHz GPR profile overlain by interpreted trench cross-section.

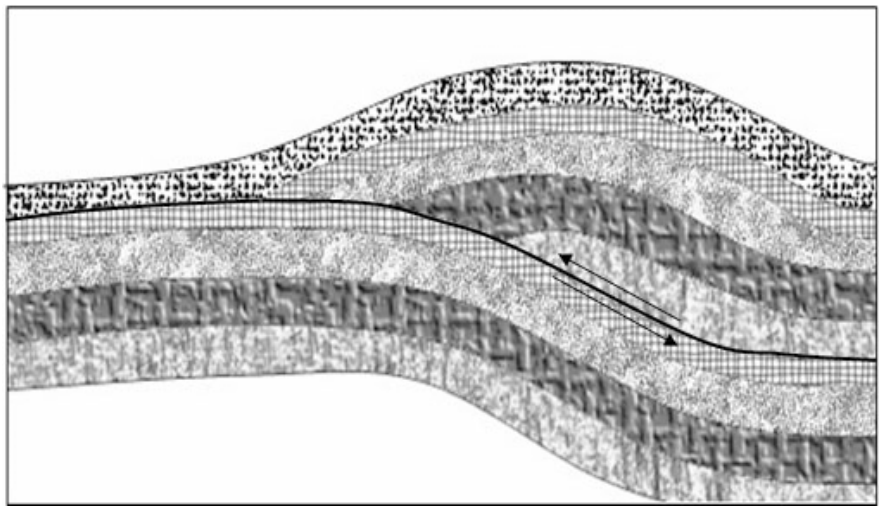

Figure 29. Large-scale thrust fault occurring from ~200 – 450 ns.

Statistical T-Test

To compare the GPR profiles with the internal structure of the trench, a statistical comparison must be accomplished. Three series of t-tests were employed, dividing the profiles into 25 ns, 50 ns, and 100 ns vertical layers per series. Each series was then analyzed using the trench as the control group and the 25 MHz, 50 MHz, and 100 MHz antennas as the groups to be tested, and using a minimum feature length of 2 m, 5 m, and 10 m, respectively. Figure 30 shows a representation of the trench, dividing the 25 MHz GPR profile interpretation (black) and the trench interpretation (red) into 25 ns layers, creating the basis for a total of nine t-tests, each to prove whether GPR is a viable tool for imaging the interior of a rock glacier.

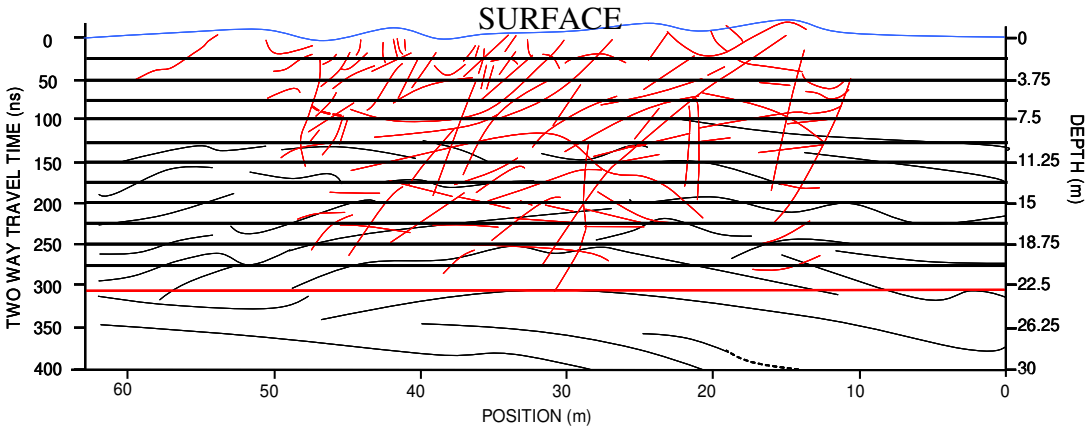

Figure 30. Example of 25 ns vertical partitioning of trench and 25 MHz GPR interpretations.

For the first series of tests, interpretations of the trench and GPR profiles were divided vertically into sections 25 ns thick, resulting in 12 partitions. The number of visible structures extending at least 2 m into each section was noted. The process was repeated with the 25, 50, and 100 MHz radar data. The results are shown in Table 3. The panoramic photograph of the trench reveals 219 total structural events, whereas the 25 MHz data showed 30, the 50 MHz data showed 90, and the 100 MHz data showed 247. With these values, a statistical t-test was conducted.

The results for the 25, 50, and 100 ns statistical comparisons are shown in Table 4, 5, and 6, respectively, including the mean, median, mode, t-value, standard error of difference, standard deviation, range, P-value, 95 % confidence interval, and results of the comparison tests. The mean is the standard average of a data set, the median is the middle of a distribution, and the mode is the value that has the largest number of

Table 3. Comparison of observable structure > 2 m within trench and GPR profiles with 25 ns vertical increments.

Depth in nanoseconds (ns)	Photograph 25 ns	25 MHz GPR 25 ns	50 MHz GPR 25 ns	100 MHz GPR 25 ns
0 - 25	19	0	0	16
25 - 50	35	0	0	33
50 - 75	28	0	4	36
75 - 100	23	0	11	31
100 - 125	23	1	10	29
125 - 150	24	6	13	28
150 - 175	15	4	11	18
175 - 200	17	3	9	14
200 - 225	15	4	7	15
225 - 250	10	4	9	18
250 - 275	6	4	9	7
275 - 306	4	4	7	2
Total	219	30	90	247

occurrences. In a normally distributed set of data, the mean, median, and mode are equivalent. For this study, a normal distribution is assumed. The standard error of difference is a statistical index of the probability that a difference between the statistical means of two samples is greater than zero (Ott and Longnecker, 2001). Standard deviation is a measure of the dispersion or variation in a distribution, the range of a data set is the difference between the highest and lowest values, and the P-value is the probability that a difference between two groups occurred by chance rather than a true relationship between measures. Confidence interval quantifies the uncertainty in a measurement. Reported as 95% CI, this stands for the range of values within which we can be 95% sure the true value lies.

Using equations 5, 6, and 7, the 25 MHz analysis had a calculated t-value of 5.873. Employing a t-table (Ott and Longnecker, 2001), the P-value was established with degrees of freedom equaling 22 and a significance level (α) of 0.05. The P-value equals 0.0001, which is much less than 0.05. Therefore, the null hypothesis is rejected, and the

Table 4. Results of the statistical t-test for 25 ns increments and structures greater than 2 m.

	25 MHz GPR vs Trench	50 MHz GPR vs Trench	100 MHz GPR vs Trench
Mean	2.5	7.5	20.583
Median	4.5	9	18
Mode	4	9	18
t value	5.873	3.74	0.576
SED	2.682	2.878	4.048
SD	2.15	4.2	10.72
Variance	4.64	17.55	115
Range	4	10	34
P-Value	0.0001	0.0011	0.5702
95% CI	10.187 to 21.3130	4.7824 to 16.7176	-10.72813 to 6.06213
Results	Statistically significant	Statistically Significant	Not Statistically Significant

Table 5. Results of the statistical t-test for 50 ns increments and structures greater than 5 m.

	25 MHz GPR vs Trench	50 MHz GPR vs Trench	100 MHz GPR vs Trench
Mean	2.67	8.5	11.33
Median	3.5	9.5	11.5
Mode	0, 4	N/A	10
t value	3.7839	0.4752	0.7866
SED	1.85	2.455	2.119
SD	2.16	4.51	3.33
Variance	3.9	16.92	9.22
Range	5	13	9
P-Value	0.0036	0.6449	0.4497
95% CI	2.88 to 11.12	-4.30 to 6.64	-6.39 to 3.05
Results	Statistically Significant	Not Statistically Significant	Not Statisically Significant

Table 6. Results of the statistical t-test for 100 ns increments and structures greater than 10 m.

	25 MHz GPR vs Trench	50 MHz GPR vs Trench	100 MHz GPR vs Trench
Mean	4.67	7	6.67
Median	6	8	6
Mode	N/A	N/A	N/A
t value	0.53	0.1754	0.1562
SED	3.145	3.801	2.134
SD	4.16	5.57	1.15
Variance	17.33	31	1.33
Range	8	11	2
P-Value	0.6242	0.8693	0.8835
95% CI	-7.06 to 10.40	-11.22 to 9.89	-6.26 to 5.59
Results	Not Statistically Significant	Not Statistically Significant	Not Statistically Significant

25 MHz GPR profile is statistically different than the cross-section of the trench. The 50 MHz analysis had a t-value of 3.74, and a P-value of 0.0011. Thus, the GPR profile is statistically different than the trench and the null hypothesis is again rejected. The 100 MHz GPR investigation had a calculated t-value of 0.576 and a P-value of 0.5702. The P-value of this comparison is large enough to not reject the null hypothesis and say that the comparison is not statistically significant.

The second series of tests utilized a 50 ns vertical partitioning of the trench and the GPR profiles. This created 6 vertical layers for analysis. Structures and foliation with lengths greater than 5 m were counted within each division. The results are shown in Table 7. The trench had 58 features greater than 5 m, the 25 MHz profile had 16, the 50 MHz profile had 51, and the 100 MHz profile had 68. Using these values, the t-test was evaluated.

Table 7. Comparison of observable structure > 5 m within trench and GPR profiles with 50 ns vertical increments.

Depth in nanoseconds (ns)	Photograph 50 ns	25 MHz GPR 50 ns	50 MHz GPR 50 ns	100 MHz GPR 50 ns
0-50	8	0	0	10
50-100	14	0	8	10
100-150	13	5	11	13
150-200	9	4	13	14
200-250	11	4	9	15
250-306	3	3	10	6
Total	58	16	51	68

The t-test was employed for a statistical comparison of the trench versus the GPR profiles using a 50 ns layering system. In the 25 MHz GPR analysis, the t-value was 3.7839. Using a significance level of 0.05 and degrees of freedom equaling 10, the P-value was 0.0036. This is small enough to reject the null hypothesis, and say that the two profiles are statistically significant. For the 50 MHz correlation, the t-value was 0.4752, which agrees with a P-value of 0.6449. This is greater than the significance level of 0.05 and, therefore, is large enough to not reject the null hypothesis and to be not statistically significant. For the 100 MHz profile, the t-value was determined to be 0.7866 and the corresponding P-value was 0.4497. The P-value for this comparison is large enough not to reject the null hypothesis, and conclude that it is not statistically significant.

The final t-test was conducted using 100 ns layering of the trench and GPR profiles, producing 3 vertical sections for comparison. Structures that measured 10 m or greater were counted. The results are shown in Table 8. The photograph interpretation had 19 structures greater than 10 m, the interpreted 25 MHz GPR profile had 14, the 50 MHz profile had 21, and the 100 MHz profile had 20. The t-test was calculated using these data.

Table 8. Comparison of observable structure > 10 m within trench and GPR profiles with 100 ns vertical increments.

Depth in nanoseconds (ns)	Photograph 100 ns	25 MHz GPR 100 ns	50 MHz GPR 100 ns	100 MHz GPR 100 ns
0-100	6	0	1	6
100-200	10	6	8	8
200-306	3	8	12	6
Total	19	14	21	20

The t-test was utilized for a statistical comparison of the trench versus the GPR profiles using 100 ns layering system for the final series of analyses. For the 25 MHz GPR analysis, the t-value was 0.53. Using a significance level of 0.05 and degrees of freedom equaling 10, the t-value corresponds to a P-value of 0.0036; large enough not to reject the null hypothesis, concluding that the comparison is not statistically significant. For the 50 MHz correlation, the t-value was 0.1754, which agrees with a P-value of 0.8693. This is greater than the significance level of 0.05 and, therefore, is large enough to not reject the null hypothesis and to be not statistically significant. For the 100 MHz profile, the t-value was determined to be 0.1562, and the corresponding P-value was 0.8835. The P-value for this comparison is large enough to not reject the null hypothesis, and conclude that it is not statistically significant.

By employing the use of a statistical analysis, the use of GPR on a rock glacier was ground-truthed. Depending on the scale of the desired target, the correct size GPR antennas should be applied. For the first series of t-tests, a small increment of 25 ns was used to ground-truth the use of GPR. The resolution of both the 25 MHz and 50 MHz antennas caused the rejection of the null hypothesis and the comparison to be statistically

significant. However, the null hypothesis of the 100 MHz antenna was not rejected as a result of the higher resolution and ability to visualize small-scale features. In the second series of t-tests, a slightly larger depth increment of 50 ns was utilized. The only null hypothesis to be rejected for this layering thickness was for the 25 MHz antenna. Both the 50 MHz and 100 MHz radar antennas were comparable, or not statistically significant when contrasted against the trench. For the final series of t-tests, a vertical depth layering of 100 ns was used. The scale of this series was large enough for each GPR profile to be comparable to the structure seen in the trench. Thus, the null hypothesis for each test could not be rejected and the comparison was not statistically different.

When employing the use of GPR for investigating the interior structure of rock glaciers, the researcher should determine the desired level of detail. For the Mount Mestas rock glacier studied in this thesis, the 100 MHz GPR antennas showed great detail from ~3 m to ~ 23 m in depth, and proved useful for reflectors > 2 m. However, the limit of exploration depth of ~ 250 ns (37.5 m) prevented deeper reflections from being seen. The 50 MHz antennas were useful for recognizing continuous layers that exhibited strong coherency. These proved to be useful for reflection events > 5 m in length. Reflections, however, below ~ 400 ns (30 m) were not prevalent. The 25 MHz antennas proved useful for coherent events > 10 m in length. Continuous reflectors were particularly noticeable to depths greater than 500 ns (37.5 m). Also, reflections below 500 ns were able to be seen.

So, this study has proven that GPR is a useful tool in visualizing the interior structure of rock glaciers. The 100 MHz antennas clearly show small scale reflection horizons caused by a change in clast orientation and changes in composition of

subsurface material from voids filled with air to voids filled with sediment and ice. These events coincide with the structure seen in the trench. Individual clasts greater than 0.375 m were also able to be recognized as a point source in the GPR profiles. Large continuous bedding layers were observed with the 25 and 50 MHz antennas which reflect the structure seen in the trench. A large scale thrust fault was also located with the GPR. However, this was not visible in the panoramic photograph because the fault occurs below the base of the trench.

CONCLUSION

GPR has been used to examine the internal structure of several rock glaciers (Berthling et al., 2000; Degenhardt and Giardino, 2003; Sauer and Felix-Henningsen, 2004; Degenhardt et al., 2005; Farbrot et al., 2005). Data from these studies indicate continuous reflection horizons throughout the entire length of each rock glacier. These views into the interior of these landforms have aided researchers in their quests to model and explain the internal deformation and movement of these features, but a fundamental question is: how well does the GPR profile mirror the true internal structure of the rock glacier? Unfortunately, comparison of a GPR profile with the actual internal structure has not previously been undertaken. The goal of this research was to ground-truth the usefulness and accuracy of GPR as a tool to map the interior structure of a specific rock glacier. A validation of how accurate the GPR profile matches the internal structure of a rock glacier was needed to achieve this goal.

The Colorado Highway Department, in searching for a borrow source for the construction of La Veta Pass, created a trench ~ 100 m long and 23 m deep through the investigated rock glacier. This trench was used to ground-truth the use of GPR on rock glaciers. GPR surveys can be used to infer the interior structure, and thus their kinematic movement.

Ground-truthing the usefulness and accuracy of GPR to map the interior of this rock glacier required four objectives to be established:

- Map the surface morphology of the Mount Mestas rock glacier.
- View the internal structure of the rock glacier using GPR with supplemental EM data.
- Compare the GPR profile and EM data with the exposed trench.

- Confirm GPR data using statistical comparisons.

Completion of these four objectives fulfills the goal and allows answers to the stated problem regarding the accuracy of GPR in mirroring true internal structures of a rock glacier.

First, the surface morphology was mapped using two overlapping aerial photos of Mount Mestas and a stereoscope. This allowed the area to be viewed in three dimensions, permitting straightforward morphological mapping to be accomplished. Then, the internal structure was recognized with a panoramic photograph of an excavated trench through the rock glacier. GPR data were next obtained parallel with the trench using 100, 50, and 25 MHz antennas. EM profiles were subsequently taken at various depths perpendicular to the trench at the midpoint of the GPR survey lines. These data were used to supplement the GPR profiles. With the panoramic photograph, GPR data, and EM data interpretations, comparisons were made using a statistical t-test to verify the usefulness and accuracy of using GPR on rock glaciers.

The size of the desired target determines the equipment needed for a successful study. Dominant wavelength of the 25 MHz, 50 MHz, and 100 MHz antennas is 6 m, 3 m, and 1.5 m, respectively. Objects smaller than ¼ the dominant wavelength will not be resolved. The 100 MHz antennas, with a vertical resolution of 0.375 m, were proven for features greater than 2 m in length, with an exploration depth of ~ 250 ns. Because the vertical resolution is smaller than a number of clasts prevalent in the trench, separate reflectors greater could be seen in the upper ~ 100 ns of the profile. Moderately continuous reflectors could also be distinguished for depths down to the limit of exploration depth. With a vertical resolution of 0.75 m, 50 MHz antennas proved useful

for reflectors > 5 m in length. Individual clasts could not be detected; however continuous reflectors were vastly observable. Reflections could be noticed from ~ 75 ns (5.6 m) down to a maximum exploration depth of ~ 450 ns (33.75 m). The interface between the zone of aeration and permafrost was well recognized because of the high dielectric contrast in the adjacent media. 25 MHz antennas were used to view large scale objects at deeper exploration depths, with a 1.5 m vertical resolution. Interfaces between the zone of aeration, the permafrost zone, and the deeper unsaturated zone, were detected. Objects greater than 10 m could be observed, and a well defined structural style similar to a fault-propagation fold model was recognized. The low frequency of 25 MHz antennas allowed exploration depths of ~ 90 ns (6.75 m).

This study has proven that GPR is a useful tool in visualizing the interior structure of rock glaciers. The 100 MHz antennas clearly show small scale reflection horizons caused by a change in clast orientation and changes in composition of subsurface material from voids filled with air to voids filled with sediment and ice. These events coincide with the structure seen in the trench. Individual clasts greater than 0.375 m were also able to be recognized as a point source in the GPR profiles. Large continuous bedding layers were observed with the 25 and 50 MHz antennas which reflect the structure seen in the trench. A large scale thrust fault was also located with the GPR. However, this was not visible in the panoramic photograph because the fault occurs below the base of the trench.

RECOMMENDATIONS FOR FUTURE STUDY

Numerous studies of rock glaciers have employed the use of GPR (Berthling et al., 2000; Degenhardt and Giardino, 2003; Sauer and Felix-Henningsen, 2004; Degenhardt et al., 2005; Farbrot et al., 2005). But how well does the GPR profile match the actual structure of the subsurface? This research incorporates both the actual internal structure as well as the structure created by GPR profiles to evaluate the usefulness of radar surveys on rock glaciers. This thesis ground-truths the use of GPR for showing the internal structure of a rock glacier. However, there are many variables to consider when conducting a GPR survey on a rock glacier such as size, shape, geographic and topographic location, altitude, origin, activity status, ice content, and geological composition. Therefore, the accuracy of a GPR profile will deviate quite a bit from rock glacier to rock glacier. Future research is necessary to encompass all possibilities.

This study compared the lengths of coherent reflections with the structure of the trench. Future research could compare dips of coherent reflections in GPR profiles with dips of bedding, foliation, and changes in lithology. The statistical test used in this study allowed comparison of the means of two groups. Future research could also devise a method that compares the difference between counts, and fit a curve to the data, as opposed to using a straight line of the mean.

To further this research, it is necessary to conduct a study using smaller antenna sizes so reflections from the upper 5 m will be visible instead of masked by air and ground waves. A strong structural background will be helpful in the interpretation process.

REFERENCES

Arenson, L., Hoelzle, M. and Springman, S., 2002. Borehole deformation measurements and internal structure of some rock glaciers in Switzerland. Permafrost and Periglacial Processes, 13, 117-135.

Barsch, D., 1977. Nature and importance of mass-wasting by rock glaciers in alpine permafrost environments. Earth Surface Processes 2, 231-245.

Barsch, D., 1996. Rockglaciers. Indicators for the Present and Former Geoecology in High Mountain Environments, Springer, Berlin, 331 pp.

Barsch, D., Fierz, H. and Haeberli, W., 1979. Shallow core drilling and bore-hole measurements in the permafrost of an active rock glacier near the Grubengletscher, Wallis, Swiss Alps. Arctic Alpine Res., 11, 349-352.

Benedict, J.B., 1973. Origin of rock glaciers. Journal of Glaciology, 12, 520-522.

Berthling, I., Etzelmuller, B., Isaksen, K. and Sollid, J.L., 2000. Rock glaciers on Prins Karls Forland. II: GPR soundings and the development of internal structures. Permafrost and Periglacial Processes, 11, 357-369.

Birnie, R.V. and Thom, G., 1982. Preliminary observations on two rock glaciers in South Georgia, Falkland Islands dependencies. Journal of Glaciology, 28, 377-386.

Bucki, A.K., Echelmeyer, K.A. and MacInnes, S., 2004. The thickness and internal structure of Fireweed rock glacier, Alaska, U.S.A., as determined by geophysical methods. Journal of Glaciology, 50(168), 67-75.

Burger, K.C., Degenhardt, J.J., Jr. and Giardino, J.R., 1999. Engineering geomorphology of rock glaciers. Geomorphology, 31, 93-132.

Clark, M.J., 1988. Advances in Periglacial Geomorphology. Wiley, Chichester, West Sussex, U.K. 481 pp.

Cross, C.W. and Howe, E., 1905. Geography and general geology of the quadrangle in Silverton Folio. U. S. Geological Survey Geologic Folio(120), 1-25.

Degenhardt, J.J., Jr., 2002. A model for the development of a lobate alpine rock glacier in Southwest Colorado, USA: Implications for water on Mars. Ph.D. Dissertation, Texas A&M, College Station.

Degenhardt, J.J., Jr. and Giardino, J.R., 2003. Subsurface investigation of a rock glacier using ground-penetrating radar: Implications for locating stored water on Mars. Journal of Geophysical Research, 108(E4), 17:1 - 17:17.

Degenhardt, J.J., Jr., Jorgensen, W.R., Giardino, J.R., Regmi, N.R., Stokes, R. et al., 2005. Internal structure of a rock glacier on Mount Mestas, CO, using ground penetrating radar (GPR): A preliminary assessment, Sixth International Conference on Geomorphology, Zaragoza, Spain, 132.

Farbrot, H., Isaksen, K., Eiken, T., Kaab, A. and Sollid, J.L., 2005. Composition and internal structures of a rock glacier on the strandflat of western Spitsbergen, Svalbard. Norwegian Journal of Geography, 59, 139-148.

Giardino, J.R., 1976. Rock glacier movement as observed by dendogeomorphic techniques, The Nebraska Academy of Sciences, Lincoln.

Giardino, J.R., 1979. Rock glacier mechanics and chronologies: Mount Mestas, Colorado. Ph.D. Dissertation, University of Nebraska, Lincoln, 228 pp.

Giardino, J.R., 1983. Movement of ice-cemented rock glaciers by hydrostatic pressure: an example from Mount Mestas, Colorado. Zeitschrift fur Geomorphologie(NF 27), 297-310.

Giardino, J.R., 2006. Per communication: Mount Mestas rock glacier characteristics, Office of Graduate Studies, Texas A&M University, College Station.

Giardino, J.R., Lason, M.P. and Shroder, J.F., 1979. Fabric analysis of rock glaciers. Program Abstracts, AAG, Washington DC, 191.

Giardino, J.R., Shroeder, J.F. and Lawson, M.P., 1978. Movement mechanisms for ice-cemented rock glaciers. American Quaternary Association Abstracts 5:202.

Giardino, J.R. and Vick, S.G., 1987. Geologic engineering aspects of rock glaciers. Bulletin of the Association of Engineering Geologists 22 (2), In: Giardino, J.R.,

Shroder, J.F. Jr., Vitek, J.D. (Eds), Rock Glaciers. Allen and Unwin, London, 265-287.

Giardino, J.R. and Vitek, J.D., 1988. Interpreting the internal fabric of a rock glacier. Geografiska Annaler. Series A, Physical Geography, 70(1/2), 15-25.

Haeberli, W., 1985. Creep of mountain permafrost: Internal structure and flow of alpine rock glaciers: Mitteilungen der Versuchsanstalt fur Wasserban. Hydrologie und Glaziologie Nr. 77, Zurich, 142.

Haeberli, W., Huder, J., Keusen, H., Pika, J. and Rothlisberger, H., 1988. Core drilling through rock glacier-permafrost, Proceedings of the Fith International Conference on Permafrost 2, Trondheim, Norway, pp. 937-942.

Isaksen, K., Odegard, R., Eiken, T. and Sollid, J., 2000. Composition, flow and development of two tongue-shaped rock glaciers in the permafrost of Svalbard. Permafrost and Periglacial Processes, 11, 241-257.

Johnson, R.B., 1967. Rock streams on Mount Mestas, Sangre de Cristo Mountains, southern Colorado. U.S. Geol. Surv. Prof. Paper(575-D), D217-D220.

Martin, H.E. and Whalley, W.B., 1987. Rock glaciers part I: rock glacier morphology, classification and distribution. Progress in Physical Geography 11 (2), 260-282.

Neal, A., 2004. Ground-penetrating radar and its use in sedimentology: principles, problems and progress. Earth-Science Reviews, 66(3-4), 261-330.

Ostrem, G., 1971. Rock glaciers and ice-cored moraines. Geogr. Annaler, 53, 207-213.

Ott, L.R. and Longnecker, M., 2001. An Introduction to Statistical Methods and Data Analysis. Wadsworth Group, Pacific Grove, CA, 1152 pp.

Patton, H.B., 1910. Rock streams of Veta Peak, Colorado. Bull. Geol. Soc. Am., 21, 663-676.

Potter, N.J., 1972. Ice-cored rock glacier, Galena Creek, northern Absaroka Mountains, Wyoming. Geological Society of America Bulletin, 83, 3025-3058.

Prost, G.L., 2001. Remote Sensing for Geologists. Taylor & Francis, Philadelphia, 462 pp.

PulseEKKO, R., 1996. User's guide version 1.2: Sensor's & Software: Technical Manual 25.

Richmond, G.M., 1962. Quaternary stratigraphy of the La Sal Mountains, Utah, U.S.Geological Survey Professional Paper 324. U.S. Government Printing Office, Washington, D.C.

Sass, O. and Wollny, K., 2001. Investigations regarding alpine talus slopes using ground-penetrating radar (GPR) in the Bavarian Alps, Germany. Earth Surface Processes and Landforms, 26, 1071-1086.

Sauer, D. and Felix-Henningsen, P., 2004. Application of ground-penetrating radar to determine the thickness of Pleistocene periglacial slope deposits. Journal of Plant Nutrition and Soil Science, 167, 752-760.

Sharma, P.V., 1997. Environmental and Engineering Geophysics. Cambridge University Press, Cambridge, U.K., 475 pp.

Sheriff, R.E. (Editor), 1977. Limitations on resolution of seismic reflections and geologic detail derivable from them. Seismic Stratigraphy - Applications to Hydrocarbon Exploration. AAPG Mem, 16, 3-14 pp.

Wahrhaftig, C. and Cox, A., 1959. Observations on rock glaciers in the Alaska Range (Abs.). Geological Society of America Bulletin, 65, 1353.

Zurawek, R., 2002. Internal structure of a relict rock glacier, Sleza Massif, southwest Poland. Permafrost and Periglacial Processes, 13, 29-42.

VITA

William Revis Jorgensen
The Department of Geology and Geophysics
c/o Dr John R. Giardino
Texas A&M University
College Station, TX 77843-3115

EDUCATION

Texas A&M University, College Station, TX

M.S. in Geology May 2007
B.S. in Geology August 2004
B.S. in Geophysics May 2004

EXPERIENCE

8/04-5/06 GRADUATE RESEARCH ASSISTANT for Dr. John R. Giardino
Texas A&M University, Geology / Geophysics Department

PRESENTATIONS AND ABSTRACTS

A Preliminary Assessment of the Validity of Ground Penetrating Radar (GPR) For Showing Internal Structure of a Rock Glacier, Mt Mestas, CO (2005 TAMU Pathways to the Doctorate Symposium; Poster Presentation)

Internal Structure of a Rock Glacier on Mount Mestas, CO, Using Ground Penetrating Radar (GPR): A Preliminary Assessment (GSA Annual Meeting and Exposition; Oral Presentation)

The Glacial Landscape of Yankee Boy Basin, CO: Initial Mapping of Landforms (TAMU Student Research Week, March 29-April 1, 2005, College Station, TX)

Enhancing the US Forest Service's Stream Reach Inventory and Channel Stability Evaluation System: A Lesson from the San Miguel River, San Juan Mountains, Colorado (TAMU Water Week, Feb 7-11, 2005, College Station, TX)

Initial Mapping of Glacial and Associated Landforms: Yankee Boy Basin, CO, USA (TAMU Pathways Research Symposium, October 15-16, 2004, Corpus Christi, TX)

MEMBERSHIPS

Geological Society of America (GSA)
Society of Exploration Geophysicists (SEG)